AD-A094 809 ARMY ELECTRONICS RESEARCH AND DEVELOPMENT COMMAND WS--ETC F/G 3/3
SOLAR ECLIPSE (1979). PART II. INITIAL RESULTS FOR IONIZATION S--ETC(U)
OCT 80 M G HEAPS, R O OLSEN, K D BAKER

UNCLASSIFIED ERADCOM/ASL-TR-0069 NL

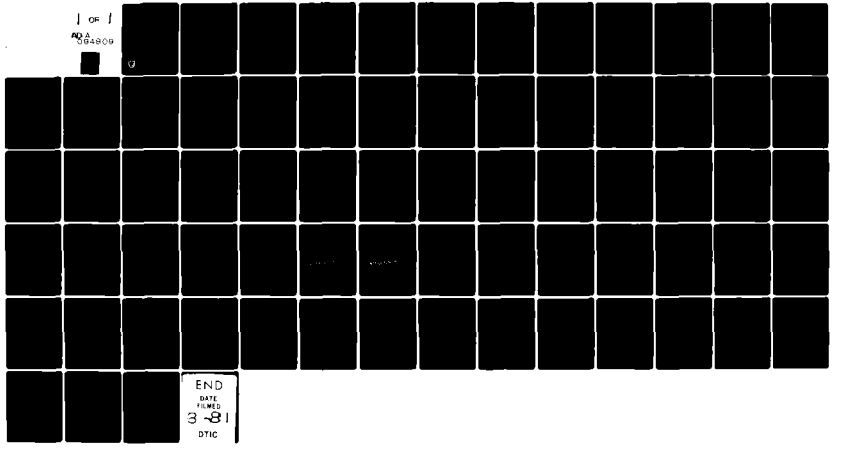

LEVEL II

ASL-TR-0069

AD

Reports Control Symbol
OSD 1366

AD A094809

1979 SOLAR ECLIPSE PART II: INITIAL RESULTS FOR IONIZATION SOURCES, ELECTRON DENSITY, AND MINOR NEUTRAL CONSTITUENTS

OCTOBER 1980

By

M. G. HEAPS
R. O. OLSEN

US Army Atmospheric Sciences Laboratory
White Sands Missile Range, NM

K. D. BAKER
D. A. BURT
L. C. HOWLETT
L. L. JENSEN
E. F. POUND
G. D. ALLRED

Space Measurements Laboratory
Utah State University, Logan, UT

US Army Electronics Research and Development Command
ATMOSPHERIC SCIENCES LABORATORY
White Sands Missile Range, NM 88002

NOTICES

Disclaimers

The findings in this report are not to be construed as an official Department of the Army position, unless so designated by other authorized documents.

The citation of trade names and names of manufacturers in this report is not to be construed as official Government indorsement or approval of commercial products or services referenced herein.

Disposition

Destroy this report when it is no longer needed. Do not return it to the originator.

SECURITY CLASSIFICATION OF THIS PAGE *(When Data Entered)*

REPORT DOCUMENTATION PAGE	READ INSTRUCTIONS BEFORE COMPLETING FORM
1. REPORT NUMBER: ASL-TR-0069	2. GOVT ACCESSION NO.: AD-A094 809
3. RECIPIENT'S CATALOG NUMBER	
4. TITLE *(and Subtitle)*: 1979 SOLAR ECLIPSE: PART II INITIAL RESULTS FOR IONIZATION SOURCES, ELECTRON DENSITY, AND MINOR NEUTRAL CONSTITUENTS	5. TYPE OF REPORT & PERIOD COVERED: R&D Final Report
	6. PERFORMING ORG. REPORT NUMBER
7. AUTHOR(s): M. G. Heaps and R. O. Olsen, ASL K. D. Baker et al, Utah State University	8. CONTRACT OR GRANT NUMBER(s)
9. PERFORMING ORGANIZATION NAME AND ADDRESS: US Army Atmospheric Sciences Laboratory White Sands Missile Range, NM 88002	10. PROGRAM ELEMENT, PROJECT, TASK AREA & WORK UNIT NUMBERS: DA Task No. 1L161102B53A
11. CONTROLLING OFFICE NAME AND ADDRESS: US Army Electronics Research and Development Command Adelphi, MD 20783	12. REPORT DATE: October 1980 13. NUMBER OF PAGES: 51
14. MONITORING AGENCY NAME & ADDRESS *(if different from Controlling Office)*	15. SECURITY CLASS. *(of this report)*: UNCLASSIFIED 15a. DECLASSIFICATION/DOWNGRADING SCHEDULE

16. DISTRIBUTION STATEMENT *(of this Report)*

Approved for public release; distribution unlimited.

17. DISTRIBUTION STATEMENT *(of the abstract entered in Block 20, if different from Report)*

18. SUPPLEMENTARY NOTES

19. KEY WORDS *(Continue on reverse side if necessary and identify by block number)*

Solar eclipse	Lower ionosphere
D region	Minor neutral constituents
Electron density	Particle precipitation

20. ABSTRACT *(Continue on reverse side if necessary and identify by block number)*

The 26 February 1979 solar eclipse provided a unique opportunity to investigate the properties of the middle atmosphere and lower ionosphere. This event served as the focal point of a cooperative field measurements program involving the US Army Atmospheric Sciences Laboratory, the Air Force Geophysics Laboratory, the National Aeronautics and Space Administration (Wallops Flight Center), and the National Research Council of Canada. This

DD FORM 1 JAN 73 1473 EDITION OF 1 NOV 65 IS OBSOLETE

SECURITY CLASSIFICATION OF THIS PAGE *(When Data Entered)*

20. ABSTRACT (Cont)

report surveys the initial data and findings of the two Army sponsored Nike-Orion rockets launched during the eclipse period. Measurements were provided of electron density, ionization sources, and critical minor constituents. The electron density profile showed a rather broad peak near 100 km with a maximum density of about 2×10^5 cm^{-3}. Measurements of ionization sources confirm the fact that during the eclipse period a particle precipitation event was in progress that largely dominated the ionization in the D and E regions. The minor neutral species $O_2(a\ ^1\Delta_g)$, OH^*, O_3, and O were monitored with atomic oxygen showing exceptionally high values in the 90 to 110 km range.

The results of the Army sponsored small sounding rocket program are presented in a companion report.

$200,000$ / cc

ACKNOWLEDGMENTS

Much of the background material which has gone into this report and much of the initial preparation for the 1979 solar eclipse field program have been performed for the Atmospheric Sciences Laboratory by the Physical Science Laboratory, New Mexico State University, and Utah State University under contract. The success of any large field program depends on the cooperation and effort of a great many people. The authors especially thank the Atmospheric Sciences Laboratory launch crews and the Utah State and Physical Science Laboratory support personnel and express appreciation for the cooperation extended by the National Research Council of Canada, the National Aeronautics and Space Administration, and the Air Force Geophysics Laboratory.

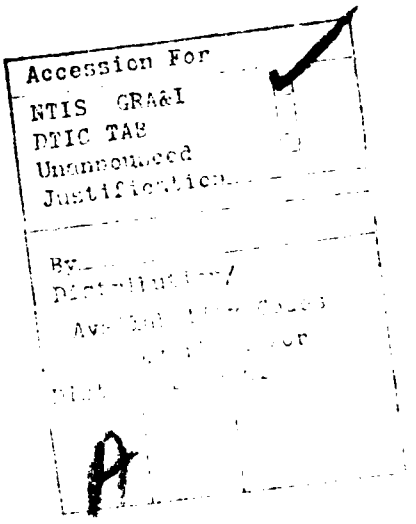

SUMMARY

The objective of the 1979 solar eclipse field measurements program has been to provide a comprehensive set of coordinated measurements in the middle atmosphere and lower ionosphere. These measurements are important for an improved understanding of the processes controlling this region and its state of ionization. This report presents the results of two Army sponsored rockets which represent a portion of these measurements.

Two closely timed measurements of electron density showed that the D region was very disturbed during the eclipse period, with electron densities of 2×10^5 cm^{-3} being measured near 90 km. A low resolution precipitating electron energy spectrum was measured, and the measurements have been converted to an ion pair production rate profile. Ionization rates for cosmic rays, solar X-rays, and Lyman-alpha radiation were also obtained, but were found to be less than the rate due to precipitating particles throughout the D region. Unfortunately, the experiment to measure NO density failed, but this failure was not as serious as it might otherwise have been because of the dominance of particle induced ionization.

CONTENTS

LIST OF TABLES

LIST OF FIGURES

1. INTRODUCTION

The basic objective of the 1979 solar eclipse field measurements program conducted 26 February 1979 at Red Lake, Ontario, Canada, was to provide measurements in the middle atmosphere of parameters crucial to an improved understanding of the chemical and physical processes controlling this region and particularly its state of ionization. To accomplish this objective, the US Army Atmospheric Sciences Laboratory (ASL) assisted in coordinating the 1979 solar eclipse field program[1] in conjunction with the National Aeronautics and Space Administration (NASA), the Air Force Geophysics Laboratory (AFGL), and the National Research Council of Canada (NRC). Rarely has such a degree of success been attained as was reached by this program. Of approximately 80 separate measurements made involving 33 sounding rockets, only a few yielded substantially less data than planned. Subsequent analyses will yield complementary sets of data from what may well prove to be the best set of coordinated middle atmospheric measurements of the 1970's.

In developing a research program for the solar eclipse, principal Army interest centered on the behavior of the ionosphere and neutral atmosphere below 100 km. Under quiet conditions, solar photon radiation is the major source of ionization above 70 km, with galactic cosmic rays providing a smaller, but dominant, source below 70 km. Under disturbed conditions, such as actually occurred during the solar eclipse period, precipitation of energetic electrons proved to be the largest source of ionization above 50 km. Experiments designed to measure in situ the several ionizing sources, electron density, and densities of several important neutral species were flown on the larger sounding rockets. (These experiments, along with those under the auspices of AFGL and NASA, constitute what is often called "the large rocket program.") Another goal of the research program was to measure numerous atmospheric parameters during the week leading up to, through, and after the eclipse, thus providing a data background during this period. The various payloads were flown with the smaller meteorological rockets. (These experiments are often called "the small rocket program.") In addition to the in situ measurements, a partial reflection sounder was operated during the entire period to provide near continuous profiles of electron densities in the D region. This report presents the initial results of the ASL sponsored portion of the large rocket program. The results of the ASL small rocket program are being reported in a companion volume.[2]

As part of the large rocket program, Utah State University (USU) and the Physical Science Laboratory (PSL) of New Mexico State University, under the

---

[1]M. G. Heaps et al, 1980, 1979 Solar Eclipse: Part I - Atmospheric Sciences Laboratory Field Program Summary, ASL-TR-0059, US Army Atmospheric Sciences Laboratory, White Sands Missile Range, NM

[2]R. O. Olsen and M. G. Heaps, 1980, 1979 Solar Eclipse: Part III - Initial Results of the Small Rocket and Partial Reflection Sounder Program, ASL-TR (in press), US Army Atmospheric Sciences Laboratory, White Sands Missile Range, NM

sponsorship of ASL, instrumented two Nike-Orion rockets that were flown during the eclipse period.[3] The two rockets, briefly denoted A_1 and B_1, were launched 30 seconds apart during the onset phase of the solar eclipse, about 25 minutes before totality. At this time some 60 percent of the solar disk was obscured. The launch summary is presented in table 1, and the payload result summary is given in table 2.

2. RESULTS OF IONIZATION MEASUREMENTS

Various measurements were made on payload B_1 to monitor different ionization sources. Energetic particles were monitored from 7 keV to 1 MeV. Cosmic rays with energies greater than 2 MeV were measured. Solar X-rays in the range of 1 to 10 keV were monitored, as well as the solar EUV and UV flux at 1216 and 2050 angstroms. It now appears certain that during the eclipse period atmospheric ionization was controlled almost exclusively by an energetic and variable flux of precipitation electrons.

2.1 Energetic Particle Precipitation

The energetic particle measurements provide a very low resolution differential energy spectrum of precipitating particles by pulse height analysis of measured particles in five approximately logarithmically related energy bins from 7 to 13, 13 to 30, 30 to 100, 100 to 300, and 300 to 1000 keV. Additionally, an integral measurement is made of all power carried by electrons between 7 keV to 1 MeV.

The measured altitude profile from each of the six electron spectrometer channels is shown in figures 1 through 6, respectively, for the ascent portion of the B_1 payload flight. Figure 1 shows the integrated power spectrum (7 keV to 1 MeV) as a function of altitude, and figures 2 through 6 show the power measured in the individual energy bins. Since the instrument was looking upward at 20 degrees with respect to normal to rocket axis and was at the same time spinning, the center of the electron spectrometer would scan over pitch angles from 36 to 74 degrees. The attitude stability of the B_1 payload was amazing. Once above the dense atmosphere, the cone angle was only on the order of 1 degree half angle and the position of the rocket axis remained also within 1 degree throughout the flight until the second stage rocket fins developed sufficient drag on descent to turn the payload over. The spectrometer field of view was made very wide (approximately 81 degrees full angle at one-half power points) to obtain maximum sensitivity; however, this field of view makes pitch angle analysis extremely ambiguous.

All of the measurements show spin modulation; however, the lower energy channels in particular have increasing modulation at decreasing altitudes. Since a good portion of the spectrometer field of view dips into negative pitch angles where particles ascend the field lines, and at low altitudes the ascending particles are increasingly unlikely, the data fit the expected behavior. At altitudes well above the deposition peak, the low energy data

---

[3]K. D. Baker et al, 1980, Rocket Measurements of D- and E-Region Parameters During the 26 February 1979 Total Solar Eclipse, Final Report under subcontract 83489 MJB, Utah State University, Logan, UT

would be considered with a very nearly isotropic pitch angle distribution over the upper hemisphere. This conclusion is invalid for the higher energy channels which appear to be consistent with a much more nearly field-aligned flux.

Very prominent, immediately noticeable features of the data are the extremely intense bursts of very high energy particles which occur randomly throughout the flight. These bursts are observed almost exclusively in the high energy channels. The 300 keV to 1 MeV channel consistently records abrupt count rate increases of about a factor of 30, lasting for a half second or so and then diminishing to a lower level after another second or two. The 100 to 300 keV channel also records these bursts, but with smaller percentage increases. Finally, the lower energy channels record these bursts as increases at altitudes below the deposition peak and as decreases above the deposition peak. Figure 7 shows a record of these bursts. In the figure the measurements are expanded between 85 and 88 seconds into the flight (95 to 98 km).

Care must be taken in inferring the causes of such decreases in the low energy component at the time of spectacular increases in the high energy component. To obtain the measurements, the spectrometer forms a pulse about 1.5μs wide which is pulse height analyzed. Very high count rates (2-3 x 10^5 counts/s) in some channels may result in apparent decreases in other channels because of instrumental pulse pileup or dead time. However, if pulse pileup or dead time were the sole cause of the observed low energy channel decreases, then the shape of those decreases would be expected to be the same in all of the low energy channels. A comparison of the decrease at 101.5 km between the 30 to 100 keV channel and the 13 to 30 keV channel illustrates that the decreases are not uniform in either size or shape. If the effects are not wholly instrumental, the data imply that the existence of a very high energy component (burst) modulates the low energy components. A tabulation of the times of high energy bursts is given in table 3. The altitude-time relationship for payload B_1 may be found from $Z = -0.004704\ t^2 + 1.872\ t - 28$, where Z is kilometers and t is seconds after lift-off.

The spectrometer pulse-height-analyzed outputs and the apparent manner in which the high energy bursts are absorbed would not be inconsistent with a monoenergetic flux of electrons in the 200 to 300 keV region which vary in time and/or space (most likely time). Electron bursts are detected as low as 55 km on descent. The burst of energetic electrons at about 101 km was seen on the RF probe as an extremely abrupt, approximately 30 percent, increase in electron density. Other features of the electron density profile have also been directly attributed to energetic electron bursts. The A_1 payload carrying an RF probe was flown 30 seconds earlier and made density measurements at some distance away. These two measurements would allow a simultaneous comparison of particle bursts and electron density perturbations at another location. Unfortunately, the A_1 payload RF probe data has had only a preliminary analysis because of an abrupt shift in the instrument zero at about 90 km on ascent.

The altitude profiles of each of the electron spectrometer channels shown in figures 1 through 6 can be used to derive the suspected primary flux of the precipitating electrons which can in turn be used to derive the ion pair

production rate profile[3] (figure 8, curve A). In calculating curve A, remember that the spectrometer channels had a low energy cutoff at 7 keV, therefore, measurements could not be made of the low energy primary flux responsible for ionization at altitudes primarily above 100 km. Curve B in figure 8 is the postulated ion pair production rate profile which would best simulate the measured electron densities. Below 90 km the profiles are identical.

2.2 Cosmic Rays

The cosmic ray detector was intended to measure cosmic ray shower products capable of depositing less than 2 MeV of energy into a 3-inch diameter, 3-inch long plastic scintillator. Since the primary cosmic ray may produce these secondary showers either in the atmosphere or in the payload itself, it becomes difficult to separate the two effects to obtain an atmospheric production rate above 20 km directly from the data. As referenced to count rates measured on the ground before the eclipse, there is no indication of unusual cosmic ray activity. The profile of count rate versus altitude is shown in figure 9 and behaves very much as expected. No further analysis is anticipated because of the apparent domination of atmospheric ionization by auroral electrons at higher altitudes.

2.3 Solar X-Rays

The measured count rates for the nominal solar X-ray energy spectrum shown in figure 10 were taken near apogee (approximately 158 km) and represent a 20-second integration of those periods of time when the instrument was directed toward the sun. A similar plot for those periods of time when the sun was outside the detector field of view is shown in figure 11. Only at the lowest energies is the dominance of the direct solar X-rays clearly discernible. At higher energies, though lower fluxes, the direct solar and nonsolar count rates are essentially the same. The origin of the counts while the sun is not within the instrument field of view has not been determined. Several possibilities exist, including: (a) precipitated energetic electrons which manage to get through the magnetic broom, (b) the Bremsstrahlung and characteristic X-rays produced as energetic electrons are stopped within both the instrument and payload, and (c) atmospheric Bremsstrahlung.

If the integrated energy carried in the direct solar flux between 1 and 10 keV is plotted as a function of altitude, the curve as shown in figure 12 results. Although some of the scatter can be attributed to counting statistics, variations in the measurements correlating with energetic electron bursts produce much of the uncertainty. When a spatial differentiation of the hand-smoothed points is performed, and if one ion pair is produced for every 35 keV of energy deposited, the ion-pair production rate shown in figure 13 is calculated.

---

[3]K. D. Baker et al, 1980, Rocket Measurements of D- and E-Region Parameters During the 26 February 1979 Total Solar Eclipse, Final Report under subcontract 83489 MJB, Utah State University, Logan, UT

Comparisons between figures 8 and 13 show that the ionization rates for the D and E regions were controlled by particle precipitation.

2.4 Solar UV (2050 Angstroms)

The solar ultraviolet detector (2050 angstroms photometer) was mounted in the payload at an angle of 25 degrees above the payload radius and was positioned to view the sun once during each payload revolution. However, the payload assumed an attitude which placed the sun near the edge of the photometer's field of view. Although the instrument worked properly, the payload experienced very little coning; and as a result, the measurements of the 2050 angstroms flux shown in figures 14 and 15 will be more difficult to interpret. Since the ionization due to electrons will be much larger than this secondary source, no additional effort is planned on these results.

2.5 Solar Lyman-alpha Radiation

The solar Lyman-alpha flux was measured on the B_1 payload by using an ionization chamber type detector. The levels of input flux measured for altitudes up to 160 km are shown in figures 16 and 17. The maximum level measured is approximately the expected irradiance level above the atmosphere for a 40 percent residual sun. The levels obtained also compare favorably with the levels of corresponding altitudes for the four Super Arcas vehicles flown in the area at other times during the the program, taking into account 60 percent reduction during the eclipse.[2]

3. RESULTS OF ELECTRON DENSITY MEASUREMENTS

Electron density measurements were provided by an RF admittance probe on both Nike-Orion rockets flown during the onset phase of the solar eclipse. Although the two payloads were launched 30 seconds apart, the results of the two are complementary, particularly since the antenna on the B_1 payload was late in stabilizing (approximately 80 km) and an electronic shift in the A_1 payload made that data not useful above 86 km. The electron density profile for the ascent portion of flight B_1 is shown in figure 18, which also shows the usable data from the A_1 flight. In the region of overlap the two results agree quite well in view of the spatial and temporal differences involved. The composite density profile rises quite rapidly from 70 to 90 km and reaches a rather broad layer around 100 km with a density of about 2×10^5 cm^{-3}. The density drops off slightly more than a factor of 2 between 110 and 125 km and then tails off only slightly up through rocket apogee of 158 km. Structure is evident in the profile, particularly the abrupt increases at 98 and 118 km.

Fine scale structure is masked in these data by the modulation resulting from the antenna, which is normal to the rocket spin axis, falling into the rarefied wake region once per spin. This effect can be noted as the thickening of the line as the rocket loses its vertical velocity approaching

---

[2]R. O. Olsen and M. G. Heaps, 1980, 1979 Solar Eclipse: Part III - Initial Results of the Small Rocket and Partial Reflection Sounder Program, ASL-TR (in press), US Army Atmospheric Sciences Laboratory, White Sands Missile Range, NM

apogee. The wake effect is much more severe as the rocket backs down on rocket descent (figure 19). In spite of this severe modulation, the general electron density profile is still useful if the modulation is ignored and the envelope of the maxima is used. This profile is similar to the ascent data; the main differences are the generally lower values above 94 km on descent, with one broad minimum at 137 km and a more distinct though narrower minimum at 115 km. Variations in the temporal and spatial aspects of the precipitating electron flux may account for such differences.

From the rather large densities observed in the D and E regions, it is apparent that substantial ionization was due to auroral particles. The profiles are representative of those accompanying auroral particles in auroral absorption events and no doubt produced the considerable radiowave absorption monitored in the vicinity of Red Lake.

4. RESULTS OF MEASUREMENTS OF MINOR CONSTITUENTS

4.1 Atomic Oxygen

The *in situ measurement of atomic oxygen*, an important minor constituent within the mesosphere and lower thermosphere, was based on the measured intensity of the 1304 angstroms oxygen resonance triplett scattered by ambient atomic oxygen from an on-board RF excited lamp. This technique offers the advantages of being sensitive and relatively free from surface recombination and gas flow rate problems. Furthermore, it is relatively unaffected by ambient pressures found in the 50 to 80 km region. Unlike other techniques, it is truly in situ and does not depend on a spatial differentiation.

The raw data in terms of detector count rate versus altitude are shown in figure 20. Interpretation of these data in atomic oxygen (O) concentrations was complicated by a number of different conditions, most important of which are:

a. High background count rates due to aurorally excited 1304 angstroms radiation;

b. Resonantly scattered solar 1304 angstroms radiation;

c. Instrument response to 2000 to 3000 angstroms solar UV;

d. High O concentrations making a large optical depth for O resonance lines within the dimensions of the scattering volume.

High backgrounds of 1304 angstroms radiation whether from solar or auroral origin increase the scatter in the measurements, since the O measurement requires a subtraction of the lamp "off" count rate from the lamp "on" count rate. If those rates are large numbers, the statistical accuracy of the difference suffers. Since the solar 1304 angstroms background must propagate downward through a medium that has large optical depth, the radiation becomes isotropic and very rapidly diminishes in intensity due to absorption (primarily by O_2) as it penetrates to about 100 km. The auroral 1304 angstroms intensity (which can have a magnitude of a kilorayleigh or so in a moderate aurora) is a function of the volume rate of energy deposition and the effective volume that the detector can see (governed primarily by absorption

by O_2). Since there was significant energy deposition from particle precipitation at all altitudes above about 80 km during the eclipse, all of the O data have somewhat more scatter than would otherwise be expected. The background count rate becomes particularly damaging at altitudes above about 110 km.

Since the background count rate near apogee was approaching the limit of the electronics, a pulse pileup produced an error and made the count rate appear smaller than it actually was. This is particularly noticeable at apogee and just below on the descent portion of the data.

Even with a "solar blind" photomultiplier and two 1304 angstroms filters, the system still has a finite sensitivity to wavelengths between 2000 and 3000 angstroms. Since there is a very significant solar intensity in this wavelength region, the detector responds to the sun on every spin once the payload is above the highly absorbing lower atmosphere. To minimize the problems from this middle ultraviolet, the data points from approximately one-third of each spin (where the direct solar effects were seen) were eliminated during analysis.

Modeling the scattering process to obtain a "transfer function," which relates count rate and atomic energy density, becomes extremely difficult as the optical depth increases within the bounds of the scattering volume and finally requires a rigorous solution as a radiative transport problem with a very difficult geometry. As a compromise, the scattering process has been evaluated in detail for each of the three oxygen resonance lines for the instrument geometry used here. Double scattering (two scattering interactions) was added with an approximation forcing the conservation of photons to partially account for effects expected by higher order scattering. The results of these calculations are shown in figure 21.

Figure 21 shows that a nonlinear saturation effect occurs at high densities and the scattering process is temperature sensitive. The nonlinearity at high densities is caused by: (1) the scattering of photons out of the beam defined by the lamp and its baffle, (2) reduction of the effective scattering cross section as the emission line becomes more and more reversed, and (3) reduction of the probability that a scattered photon will make its way back to the detector because of further scattering. The temperature dependence is due to how well the emission and absorption line shapes match (both are Doppler temperature broadened) and the temperature determined distribution of ground state levels in the absorbing oxygen atoms.

When the data are analyzed by using curves of figure 21 and the AFGL falling sphere temperature measurements on payload B_1,* the ascent and descent profiles shown in figures 22 and 23, respectively, result. The peak density measurement is in error, since even as little as a 10 percent error in any of the instrument calibrations, cross sections, or modeling of the scattering process within the measurement system geometry could produce entirely different results at the peak while making comparatively little difference at lower density portions of the flight. Undoubtedly the atomic oxygen density

---

*C. R. Philbrick, private communication, 1979

was high; best estimates of peak densities are shown by the dashed lines in figures 22 and 23. Absorption by O_2 at altitudes of 70 km and below was not considered in the analysis and will have the effect of increasing the atomic oxygen density somewhat above the measured values below 70 km. Analysis is continuing to refine the results, particularly in the high density regime.

In the absence of particle precipitation, the altitude profile of zenith 5577 angstroms atomic oxygen airglow emission is very useful as a comparison against the resonant scattering technique for the measurement of atomic oxygen as discussed earlier. In the presence of particle emission and a measured atomic oxygen profile, the 5577 angstroms emissions can provide a monitor of auroral activity and some assistance in inferring a volume ion production rate.

The measurement from the 5577 angstroms vertical viewing photometer is shown in figures 24 and 25 for ascent and descent, respectively. The large-scale variations appearing throughout the flight are periodic and correlate with the precessional period of the payload. This appears to be due to insufficient baffling against solar radiation for the altitude that the payload assumed. Since an altitude dependence was observed in the measured signal (as would be expected in penetrating an emitting layer), the minima may provide a true monitor of auroral emissions. The 5577 angstroms photometer data may be used further after the various measurements have been correlated.

4.2 $O_2(a^1\Delta_g)$, $OH^{\ddagger}$, O_3

The infrared-active minor species $O_2(a^1\Delta_g)$, $OH^{\ddagger}$, and O_3 were investigated in situ by using two techniques: the solar occultation method for ozone determination, and infrared radiometry for the $O_2(a^1\Delta_g)$ and $OH^{\ddagger}$ determinations. Unfortunately, useful data from the solar occultation experiment are very limited, although data below 40 km are a possibility if a more extensive treatment of the descent data were deemed to warrant the effort. Hence, the radiometric measurements will be emphasized in this section.

The spectral channels of the three-channel, near-infrared radiometer were centered at 1.27μm, 1.56μm, and 1.97μm, with equivalent ideal half-power bandwidths of 0.029μm, 0.21μm, and 0.23μm, respectively. The λ1.27μm channel effectively selected the atmospheric radiation associated with the (0,0) transition in the infrared atmospheric (IR At) system ($a^1\Delta_g \rightarrow X^3\Sigma_g^-$) of the O_2 molecule. Significant spectral contamination of this dayglow measurement is deemed unlikely. The bandpass of this channel included portions of the OH Meinel (7,4) and (8,5) bands, which are expected to be much weaker than the O_2 1.27μm emission at all altitudes under the conditions of the experiment. The OH Meinel (3,1) and (4,2) bands were expected to be dominant contributors to the airglow signal in the λ1.56μm channel. However, lower altitude contamination from the O_2IR At (0,1) emission at 1.58μm must be considered. The branching ratio $[I(1.27)/I(1.58)] \approx [A(0,0)/A(0,1)] \approx (40\text{-}70)$, together with the measured I(1.27), permits correction of the λ1.56μm measurements for this contamination. The λ1.97μm channel was designed to select OH Meinel $\Delta v = 2$ bands with upper vibrational quantum number $v' = 6 - 9$. Spectral contamination in this channel is expected to result primarily from the (0,0)

band of the Noxon system at λ1.91μm. The intensity of this band has been estimated to be about 2 percent that of the IR At (0,0) emission. Hence, it could contribute significantly to the signal from the λ1.97μm channel if the estimated intensity ratio is valid under the conditions of the experiment.

4.3 Radiometric Measurements--λ1.27μm Channel

High-quality data were realized from both the high- and low-gain outputs. Useful ascent data were acquired from about 68 km to 105 km, where the O_2 1.27μm signal became indistinguishable from the high-altitude background. Useful descent data were acquired from 105 km to about 60 km. However, the vehicle aspect changed markedly near T + 300 s (about 70 km), and careful aspect correction of the lower altitude data will be required.

The high-altitude signal (0.5 V peak-to-peak [high gain]) remained nearly constant from 105 km to near apogee (140 km). A 30 to 40 percent increase in signal occurred near apogee, followed by a nearly constant signal level to an altitude of 105 km on descent. This background signal was essentially independent of vehicle aspect (coning), which makes it unlikely that it is of direct solar origin. The source has not yet been identified.

Overhead emission rate profiles are presented in figures 26, 27, and 28. The results in the figures were obtained from the raw data by smoothing (0.10 s sliding average), instrumentally correcting (absolute responsivity factor), and adjusting for the effective filter transmittance for the O_2 1.27μm radiation (the filter factor does not necessarily apply to the high-altitude signal since the associated spectral distribution is unknown). The filter factor was obtained from a convolution of O_2 IR At (0,0) synthetic emission spectra with the system spectral responsivity function. Two effective rotational temperatures, 175°K and 300°K, were considered in the analysis. These temperatures bracket those of interest to the measurements. The filter factors computed at the two temperatures differed by only 1 percent. Hence, a single correction factor (1.80) was used at all altitudes.

In principle, the high-altitude background signal should be subtracted from the lower altitude results to obtain the "true" O_2 λ1.27μm overhead emission-rate profile. This step was not done in preparing the set of figures presented herein. The procedure is of little consequence in determining the volume emission rate profile from the overhead emission rate profile, since the constant is automatically eliminated in taking the derivative. Nevertheless, this correction should be kept in mind when the set of figures relating to overhead emission rates is examined.

Differential emission-rate profiles for the O_2 λ1.27μm emission are shown in figure 29. The differential emission rate (lower scale - kR/km) was converted to an $O_2(a^1\Delta_g)$ concentration by using the accepted value of 2.58×10^{-4} s^{-1} for the pertinent A coefficient. (Note that [1 kR/km] = 10^4 photons/cm^3 s.) Descent data below 80 km are suspect because of changes in viewing apsect which have not yet been fully considered. A two-layered structure in the 80 to 95 km region is suggested by both the ascent and descent data, but the evidence is not compelling at the current stage of data analysis. It should be noted that the ascent and descent profiles are essentially identical above 82 km when the descent profile is displaced downward by 1.5 km. This factor

may reflect a slight inaccuracy in the trajectory equation which was used, but the cause remains uncertain at this point.

It is now generally recognized that the upper portion (<80 km) of the $O_2(a^1\Delta_g)$ profile is quite variable, responding to significant changes in high-altitude ozone. The secondary maxima in the 80 to 95 km region apparently exhibit seasonal effects and respond to stratospheric warming events. Above 94 km, the present measurements show a very steep decline with an effective scale height of about 2.5 km.

4.4 Radiometric Measurements--OH Meinel Channels

The data from the $\lambda 1.56\mu m$ and $\lambda 1.97\mu m$ channels have not been subjected to a complete analysis. Preliminary ascent data for these channels are presented in figures 30 and 31. A problem arises in connection with the interpretation of the maximum which occurs at 98 km in the overhead radiance profiles from each of these channels.

This behavior might be attributed to an instrument malfunction; however, the descent data exhibit the same general trends as do the ascent data, thus providing a point favoring the validity of the data. The data from the $\lambda 1.97\mu m$ channel is particularly anomalous. A very low signal level occurred immediately after the pop-cover was removed from the instrument. This low signal level was followed by a fairly rapid increase to a peak value about 15 times the initial value, with a subsequent gradual decline in signal at higher altitudes to a value near apogee of approximately 3 times the initial value.

In spite of the currently uncertain interpretation of the signals from the $\lambda 1.56\mu m$ and $\lambda 1.97\mu m$ channels, some progress has been made in defining the altitude distribution of $OH^{\ddagger}$ at the time of the eclipse. The AFGL/USU liquid-helium-cooled radiometer provided good data on mesospheric OH Meinel emissions in the (1,0) and (2,1) bands. An apparent overhead emission rate of approximately 50 kR was observed at 78 km immediately after the pop-cover was removed from the instrument and the nosetip was separated. Nightglow emission levels in the (1,0) and (2,1) bands are expected to be about 150 kR and 90 kR, respectively. The data have not been corrected for the effective filter factor, but the corrected total intensity is expected to be roughly a factor of 4 below these nightglow estimates. The volume emission rate profile peaked between 85 and 86 km and had a full width at half maximum of about 6.5 km.

Several minor neutral constituents were successfully measured, with atomic oxygen showing extremely high values of 1×10^{12} cm^{-3} near 90 km. A profile for $O_2(a^1\Delta_g)$ was obtained, and a profile for O_3 below 40 km may also be extracted from the data. Several bands of $OH^{\ddagger}$ were also monitored.

These data, in conjunction with the complete set of coordinated measurements, may well represent the most comprehensive set of middle atmospheric measurements of the 1970's.

TABLE 1. 1979 SOLAR ECLIPSE SOUNDING ROCKET LAUNCH SUMMARY USU/OSL/ASL

Launch Date	Vehicle	Vehicle Identification	Launch Time (GMT)	Apogee	Measured Parameters
26 February	Nike-Orion	ASL-SE-79A_1 (A_1)	1628:00	140	Density and altitude distribution of NO, O, O_3, OH and O_2 ($^1\Delta_g$); solar lyman-alpha; electron density.
26 February	Nike-Orion	ASL-SE-79B_1 (B_1)	1628:30	158	Solar lyman-alpha; electron/proton flux and spectra; solar X-rays; cosmic ray flux (> 2 MeV); solar UV (2050 angstroms); electron density, atmospheric density/temperature (40-150 km) (AFGL).

TABLE 2. SUMMARY OF RESULTS USU/PSL PAYLOADS

A1 Payload

Instrument	Measurement	Results/Comments
Resonance lamp	O density	Good measurement. Relatively high O density. Auroral activity complicates analysis.
RF capacitance probe	Electron density	Good data up to 90 km on ascent.
Three-channel IR radiometer 1.27μm, 1.58μm, 2.1μm	O_2 ($^1\Delta_g$) OH	All channels seemed to function properly. O_2 ($^1\Delta_g$) results good. OH channels give unexpected profiles.
Lyman-alpha ionization chamber	Solar Lyman-alpha	Instrument normal. Interfering signal on telemetry necessitates hand reduction of data.
Visible photometer	OI 5577A	Instrument functioned properly. Auroral activity precludes derivation of O density by this method.
NO photometer	NO density	No usable data. Data acquisition register failed.
UV absorption photometer	O_3 density	Only low altitude data < 40 km on descent.

B1 Payload

Instrument	Measurement	Results/Comments
Proportional counter	Solar X-rays	X-ray spectra 1-10 keV.
RF capacitance probe	Electron density	Complete electron density profiles. Descent data complicated by vehicle wake effect.
Scintillation counter (electron)	Energetic electrons Total E > keV Four separate energy channels	Total energy data throughout flight. Higher than anticipated aurora saturated pulse height channels above ~ 85 km.
Scintillation counter (cosmic rays)	Cosmic ray flux	Data complete until telemetry loss at 55 km on descent.
Lyman-alpha ionization chamber	Solar Lyman-alpha flux	Good data throughout flight.
UV photometer	2050 A flux	Instrument functioned well. Rocket aspect did not allow direct solar view.

TABLE 3. TIMES OF MAJOR HIGH ENERGY ELECTRON BURSTS AS MEASURED BY THE HIGHEST ENERGY CHANNEL OF THE ELECTRON SPECTROMETER

Onset time (See after lift-off*)	Duration (s)
78.05	.8
85.4	.3
88.8	.4
96.2	.7
103.6	.4
105.4	.3
113.15	.8
142.05	.3
157.3	.3
214.05	1.0
235.4	.2
236.0	.3
237.0	.3
269.1	.3
275.6	1.2
288.9	.3
293.1	1.2
295.3	1.9
300.5	.3
302.6	1.3
304.7	.6
309.6	1.0
319.35	.8
322.7	.2
327.6	.6
330.4	1.1
333.3	1.7
337.2	.2

*Lift-off time = 1628:30 UT.

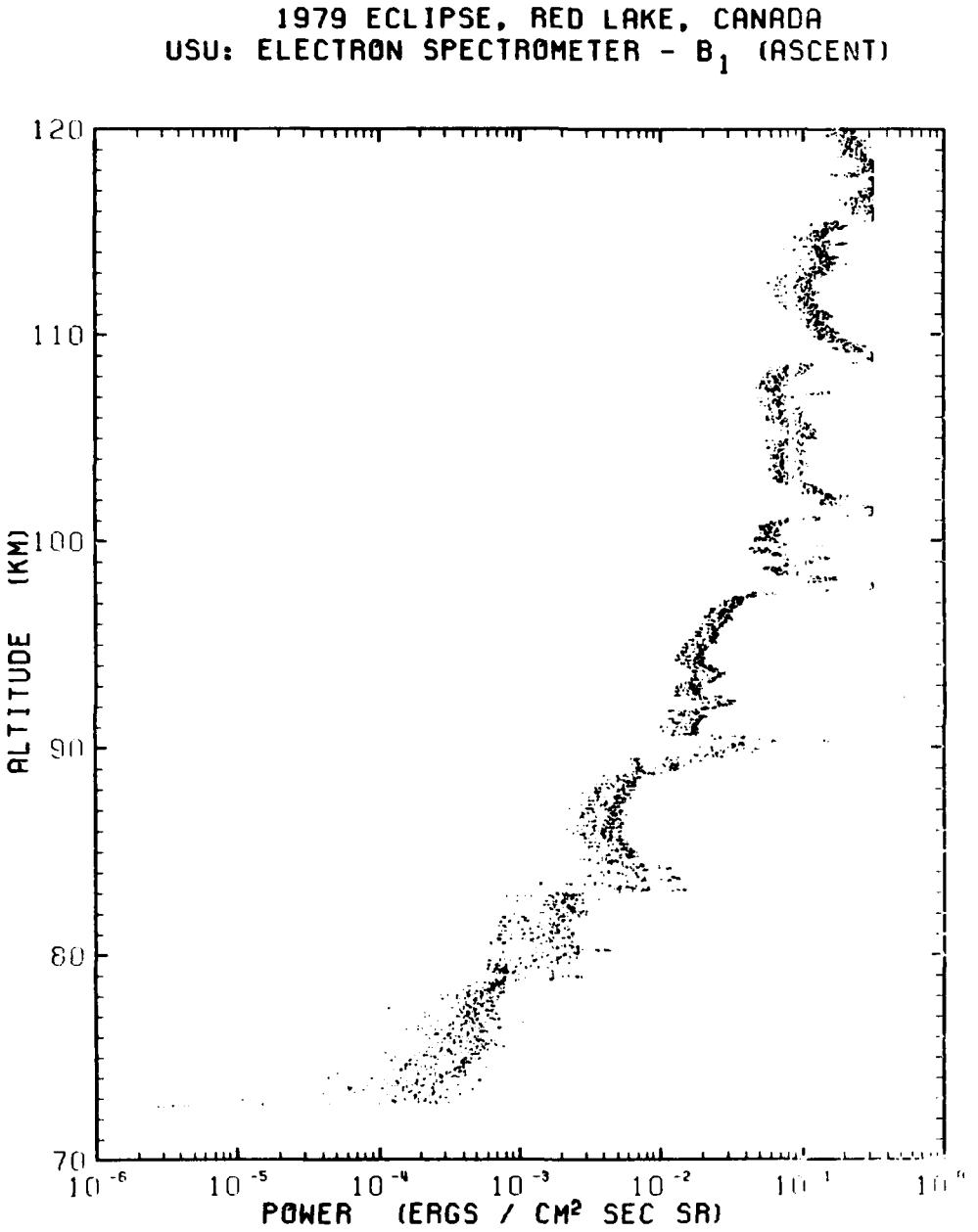

Figure 1. Altitude profile of power carried by energetic electrons from 7 keV to 1 MeV.

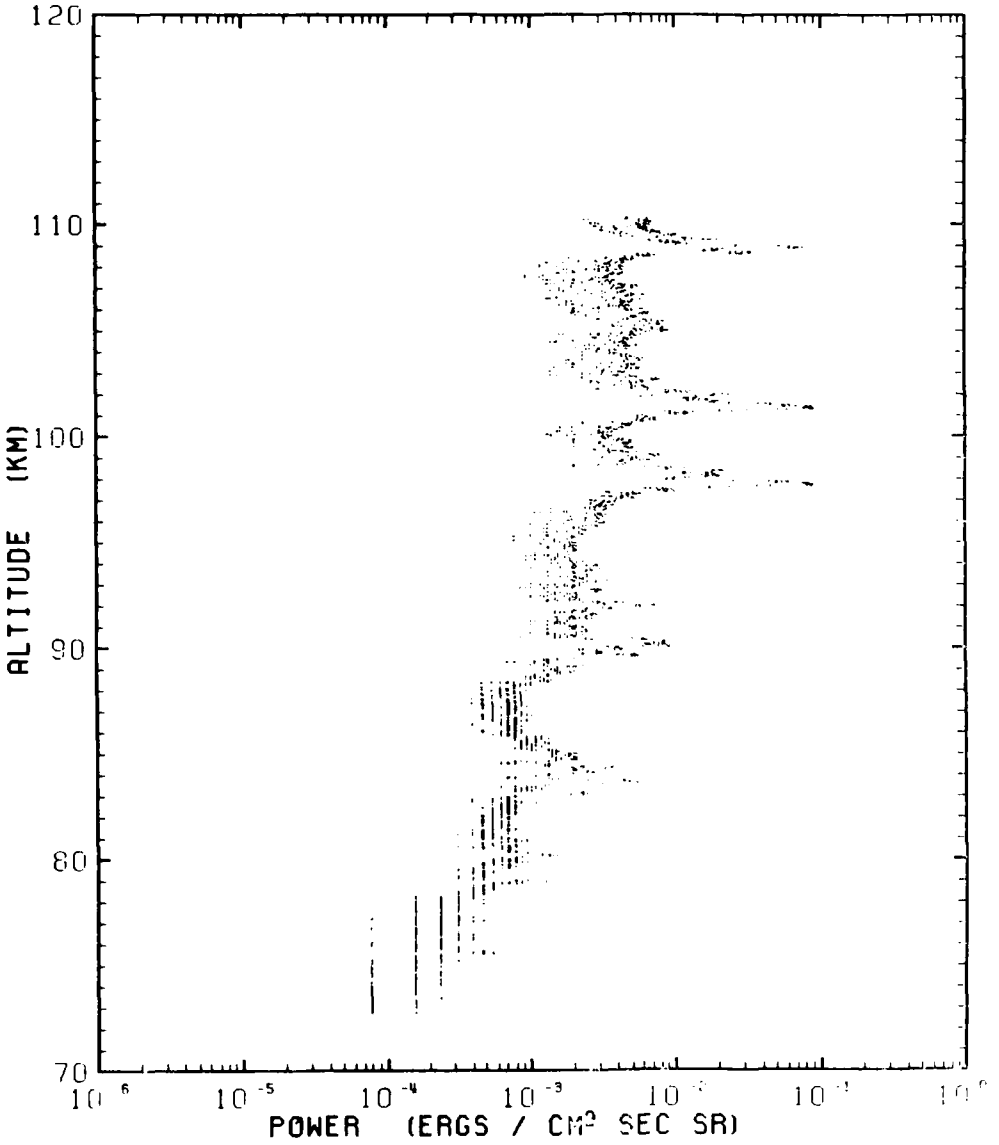

Figure 2. Altitude profile of power carried by electrons having energies between 300 keV and 1 MeV.

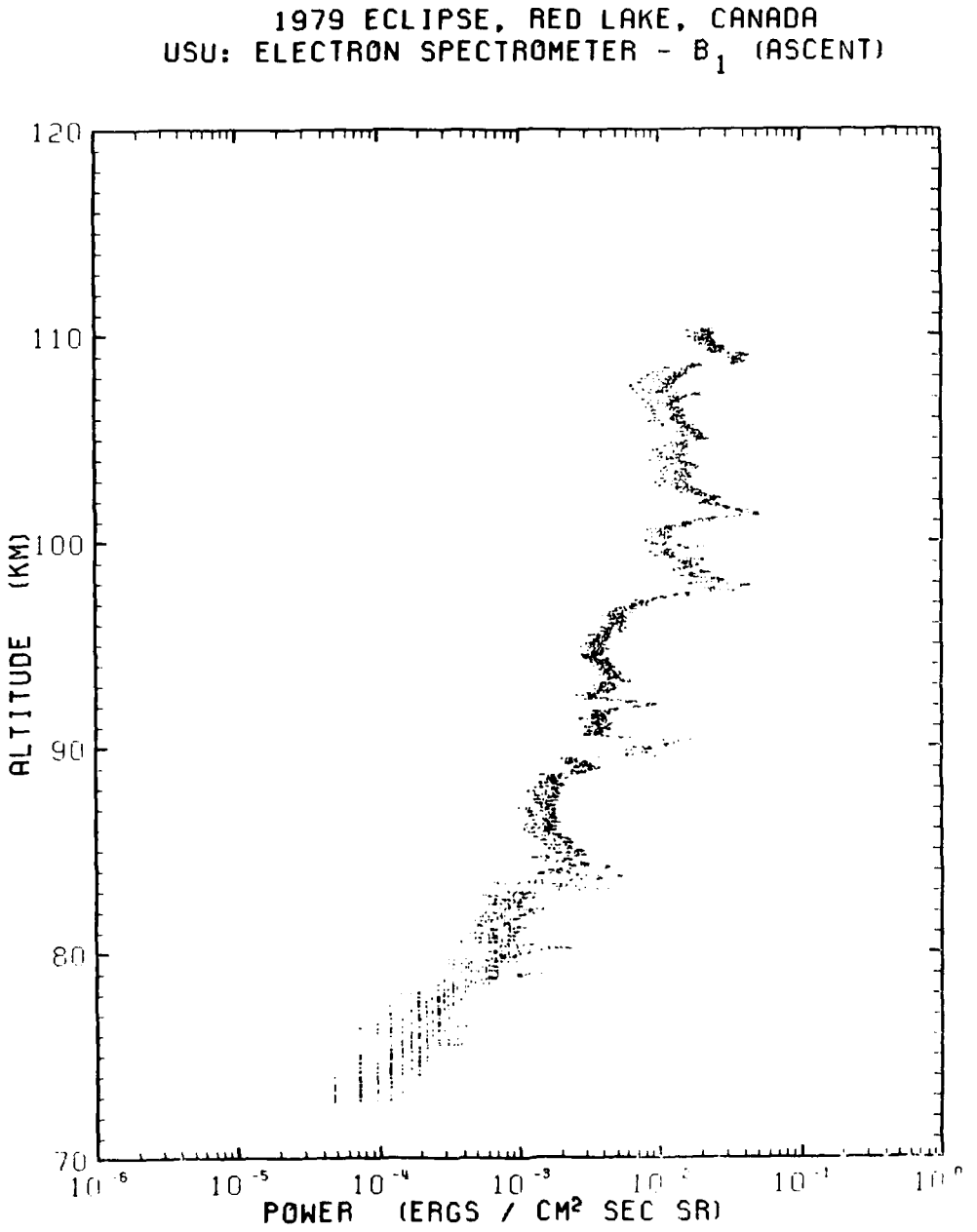

Figure 3. Altitude profile of power carried by electrons having energies between 100 keV and 300 keV.

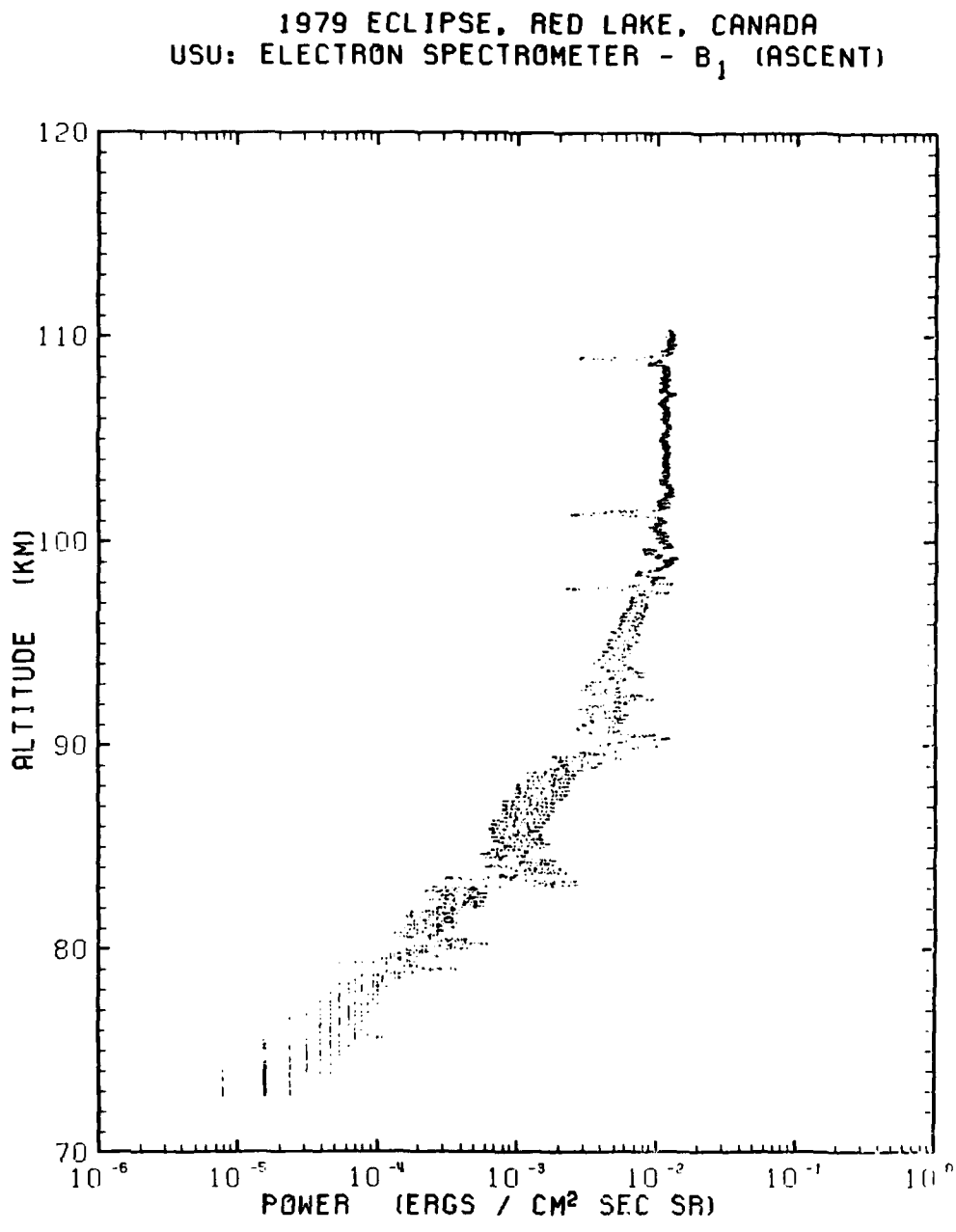

Figure 4. Altitude profile of power carried by electrons having energies between 30 keV and 100 keV.

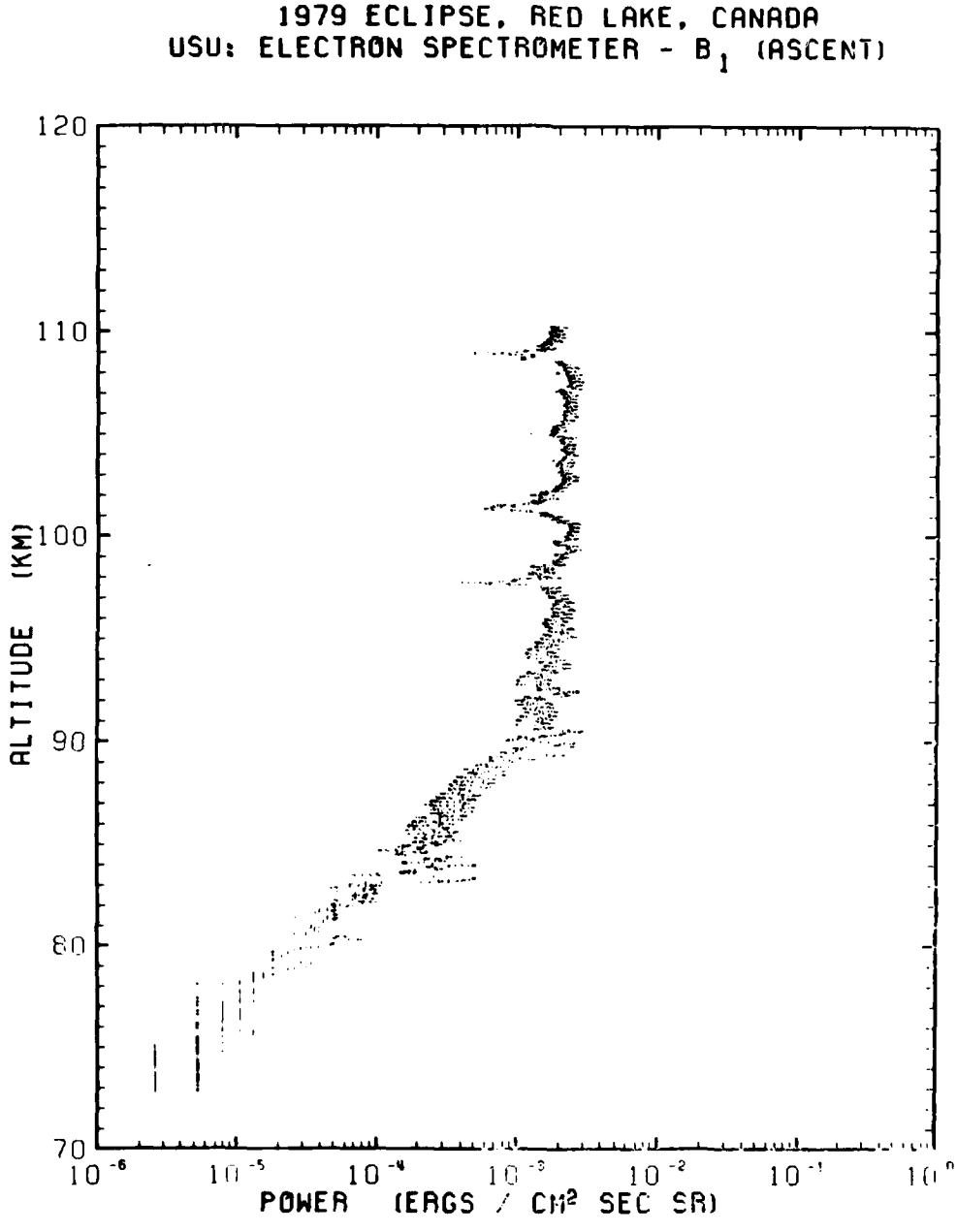

Figure 5. Altitude profile of power carried by electrons having energies between 13 keV and 30 keV.

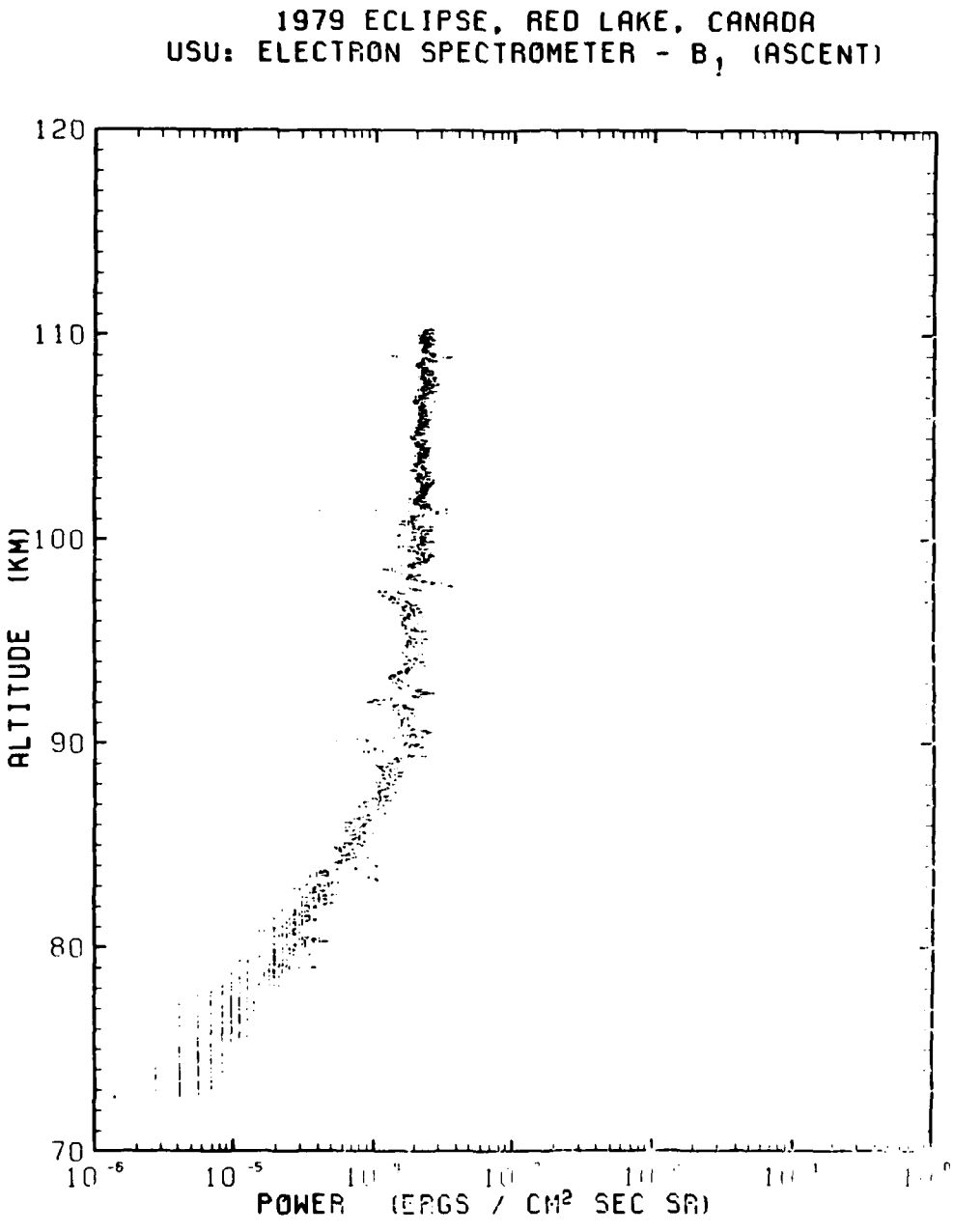

Figure 6. Altitude profile of power carried by electrons having energies between 7 keV and 13 keV.

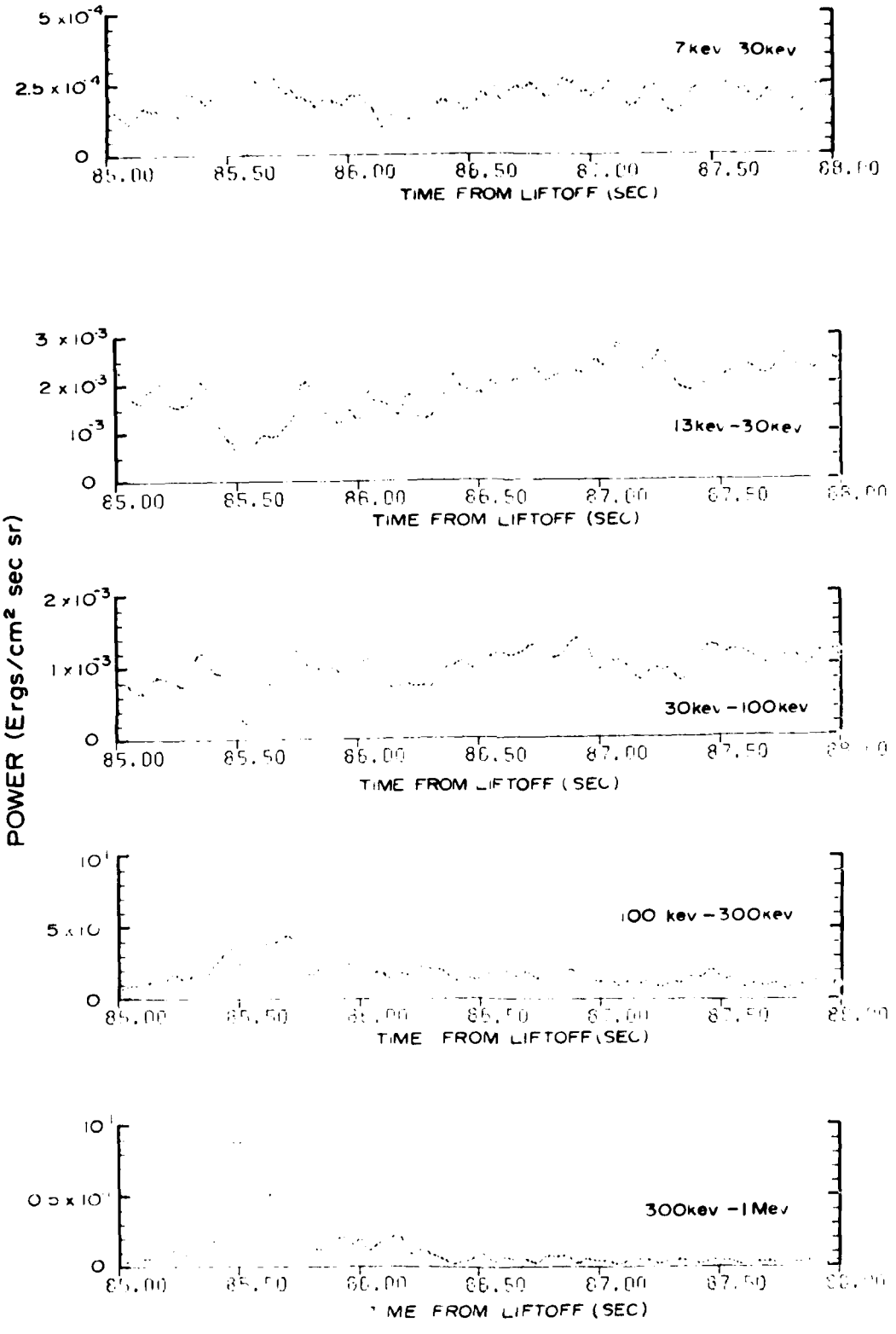

Figure 7. High energy bursts at about T + 85.5 s as seen simultaneously by all electron spectrometer energy channels.

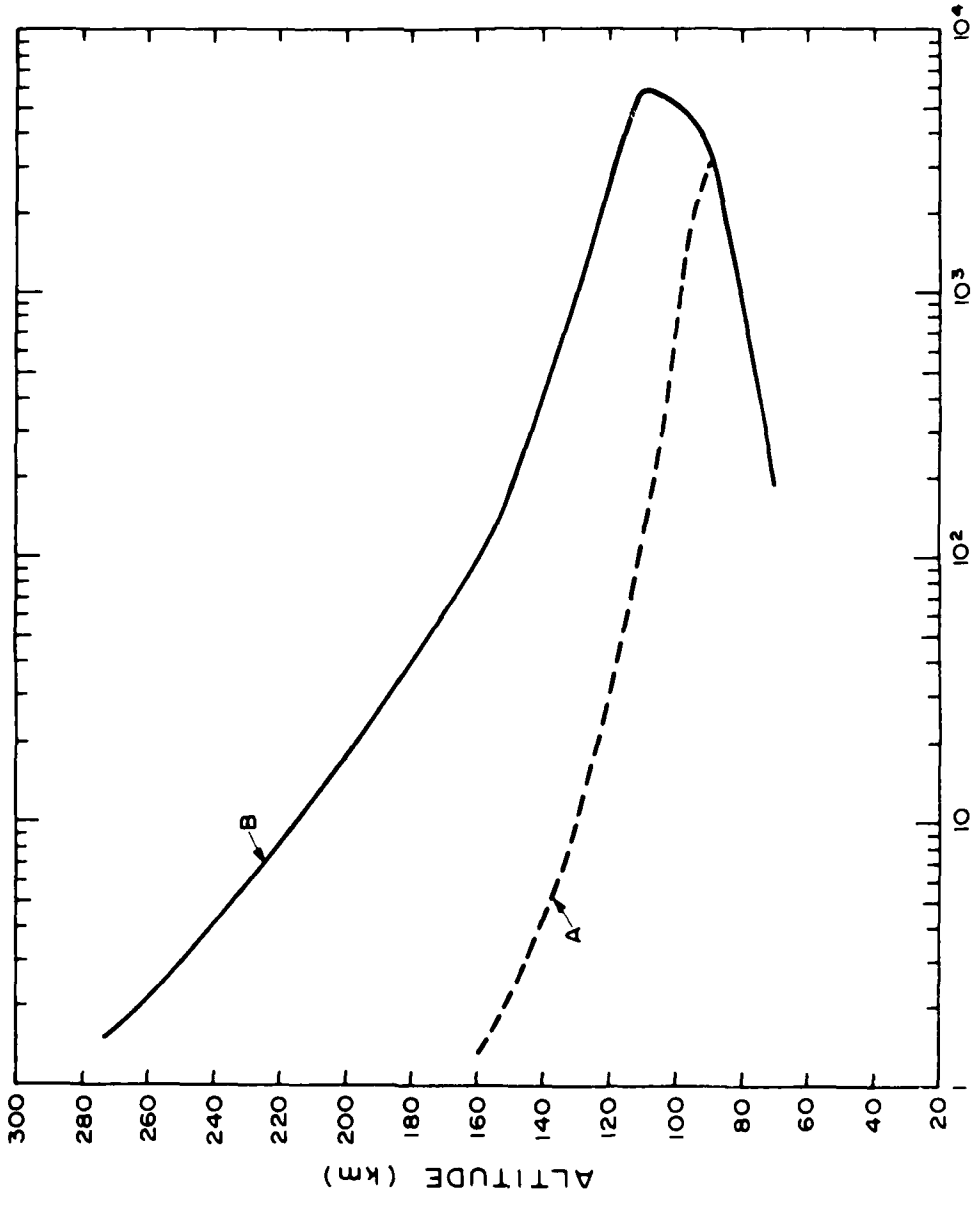

Figure 8. Ion production rate profiles for the electron flux based on the electron spectrometer (A) and inferred from the electron density data (B).

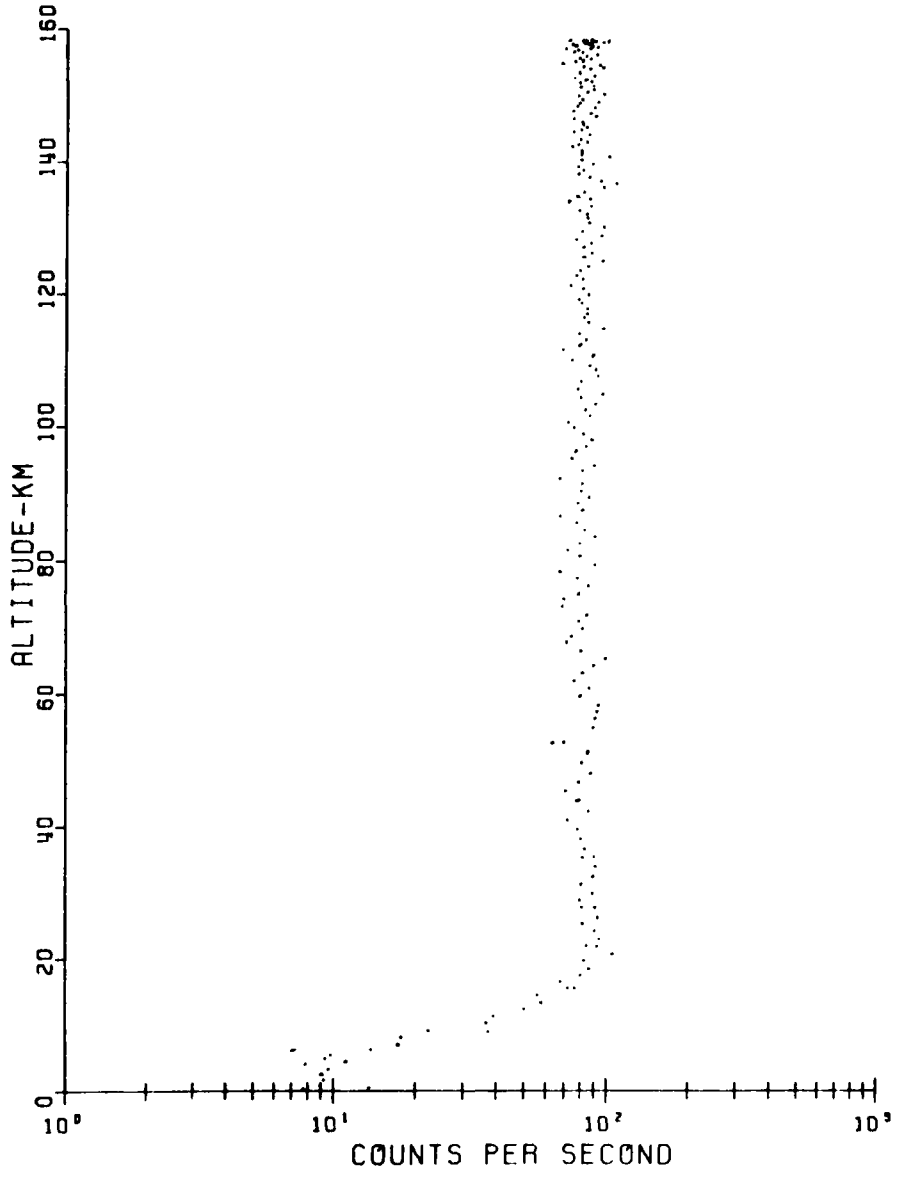

Figure 9. Altitude profile of cosmic ray detector count rate.

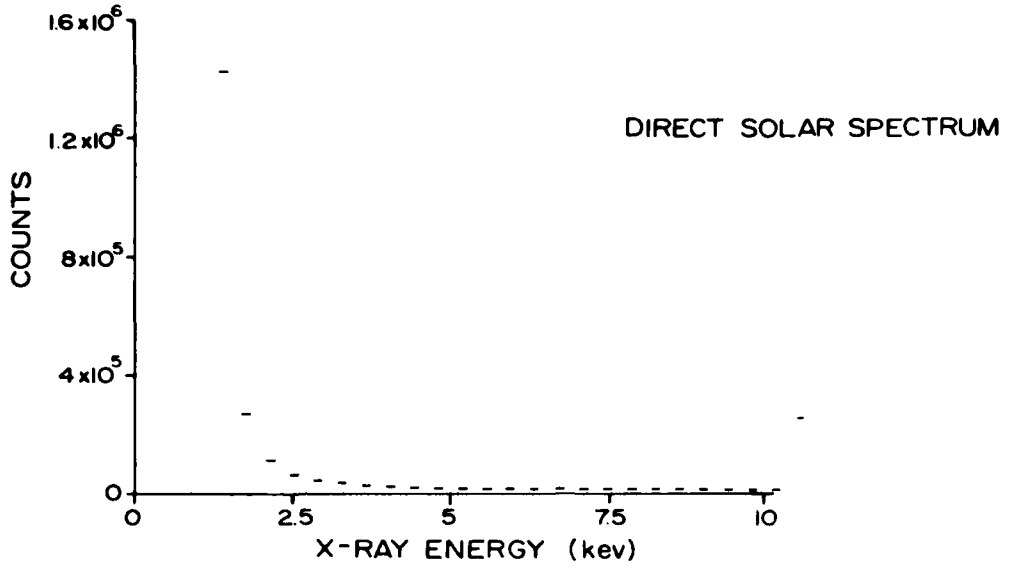

Figure 10. Measured solar direct X-ray spectrum at 158 km.

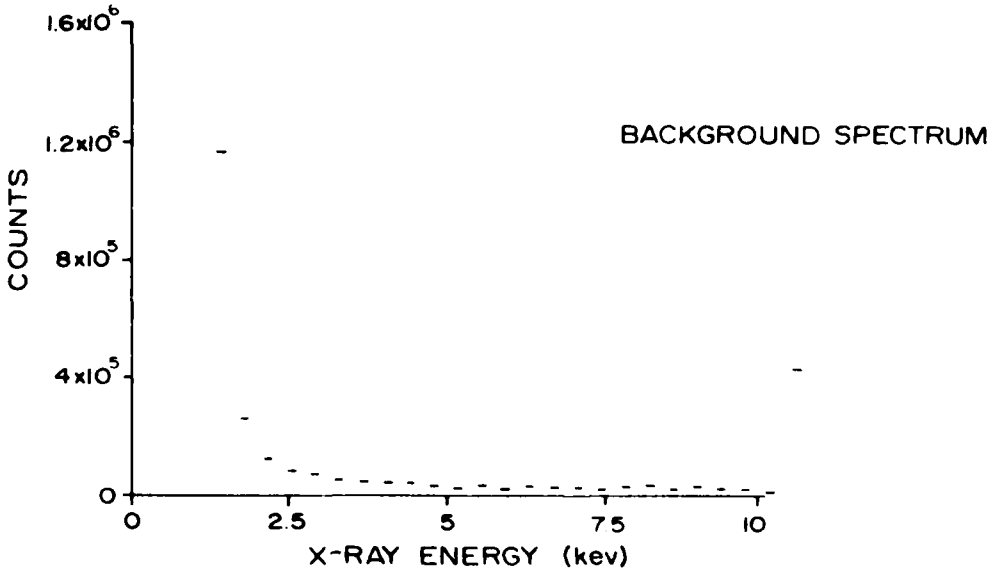

Figure 11. Measured background X-ray spectrum at 158 km.

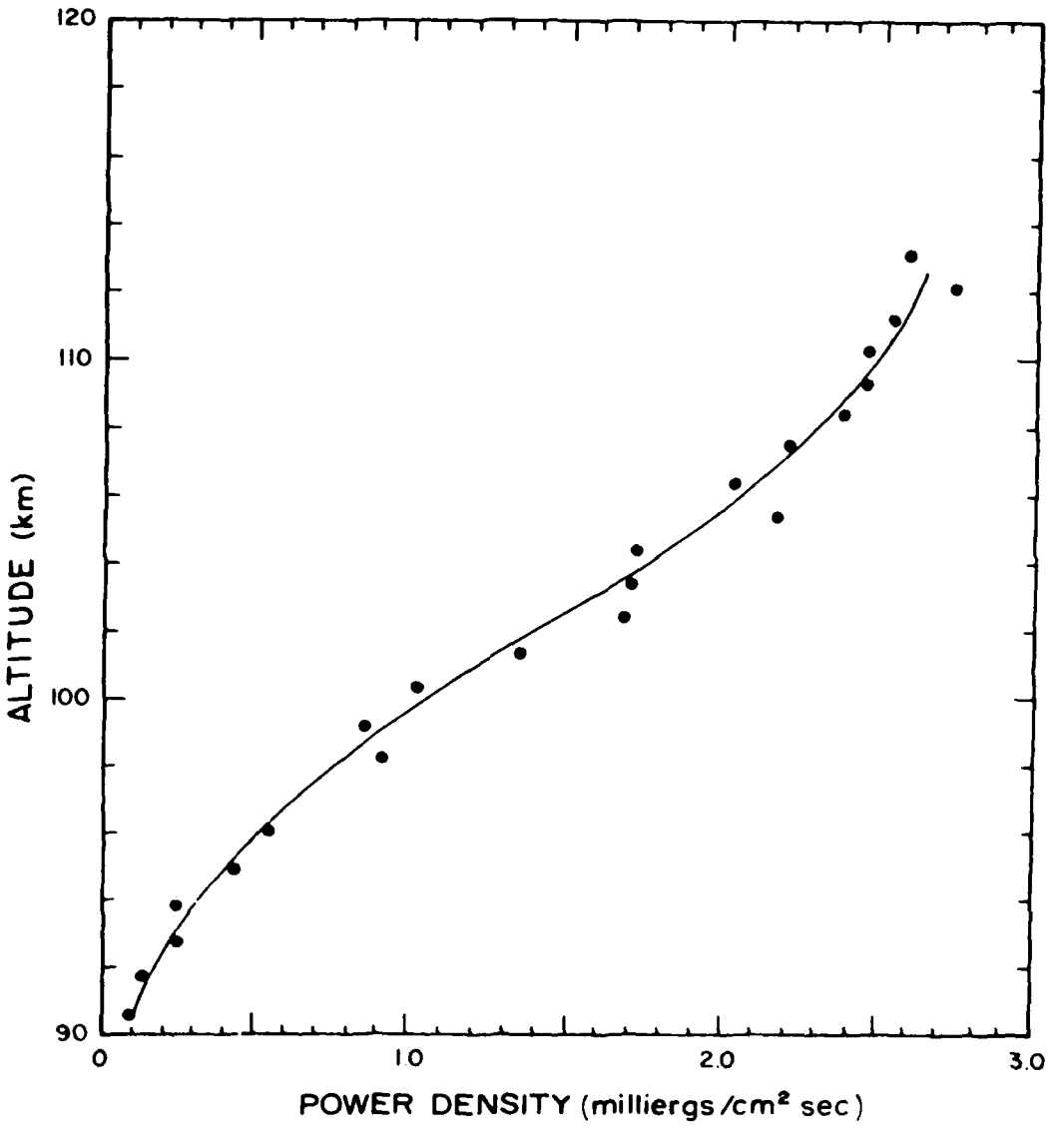

Figure 12. Altitude profile of power density from integrated solar X-ray spectrum.

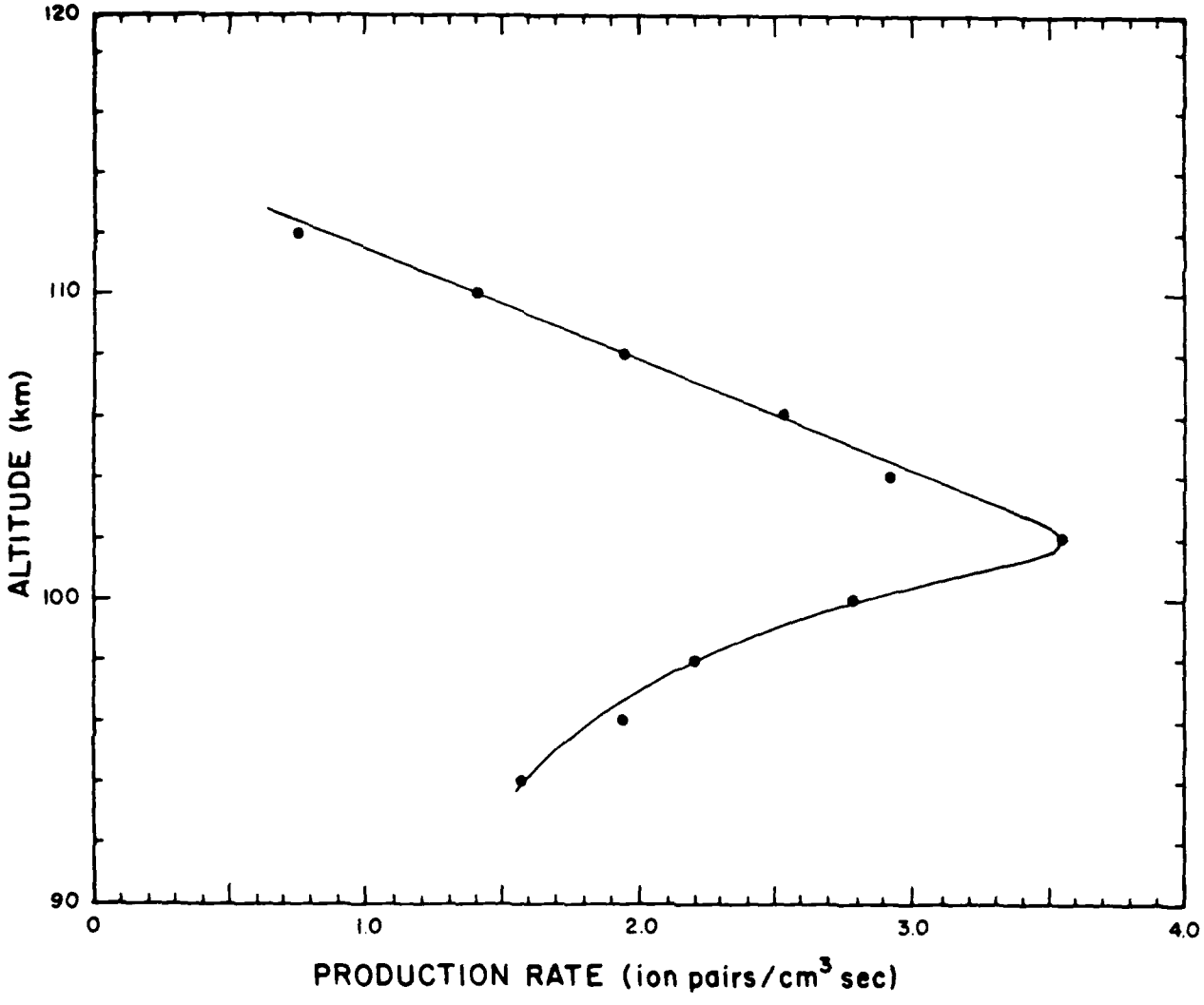

Figure 13. Altitude profile of ion pair production rate from solar X-rays assuming 35 eV per ion pair and differentiating power density profile of figure 12.

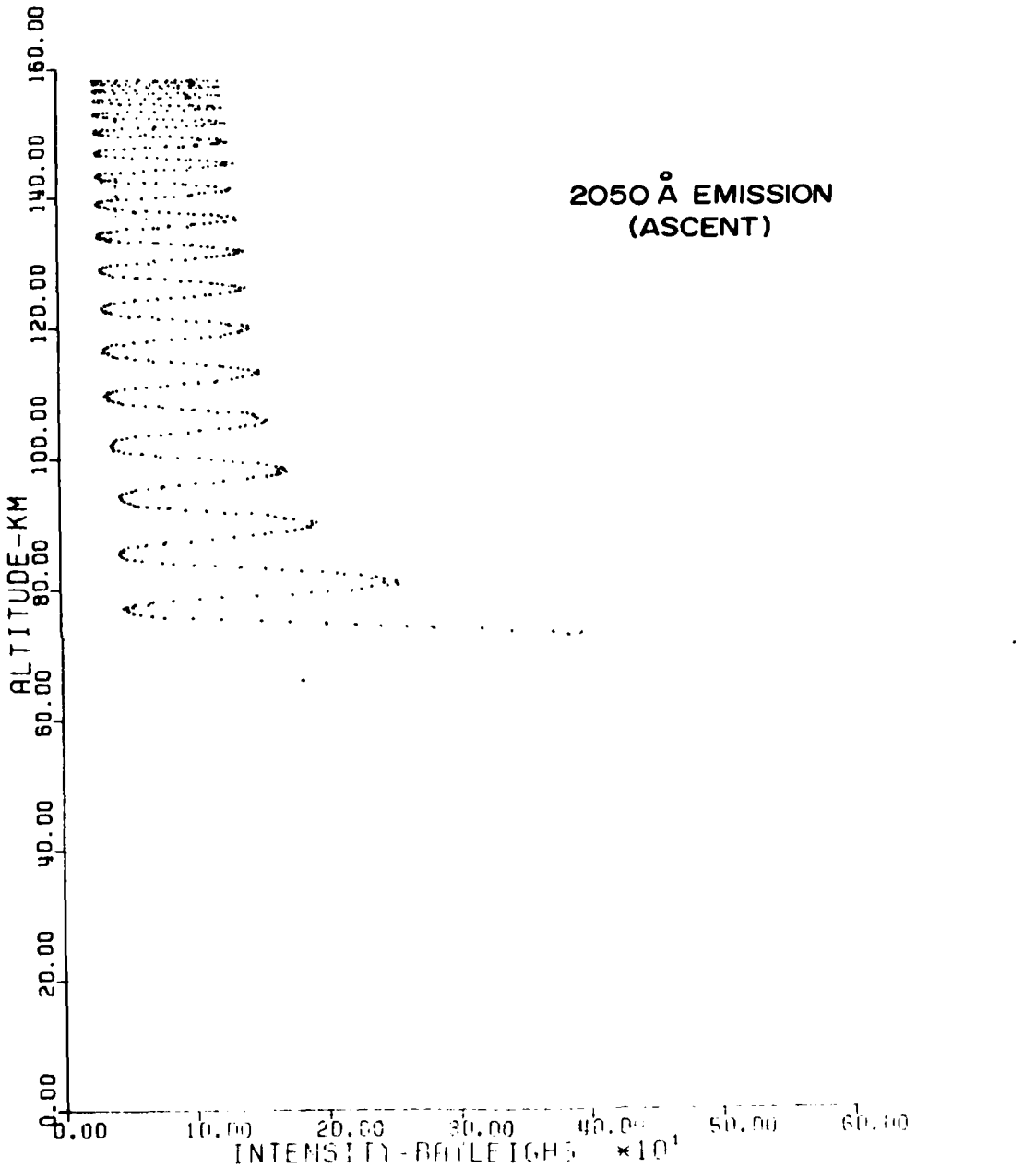

Figure 14. Ascent profile of solar 2050A intensity. The modulation is due to vehicle precession and the solar disk being at the extreme edge of the detector field of view.

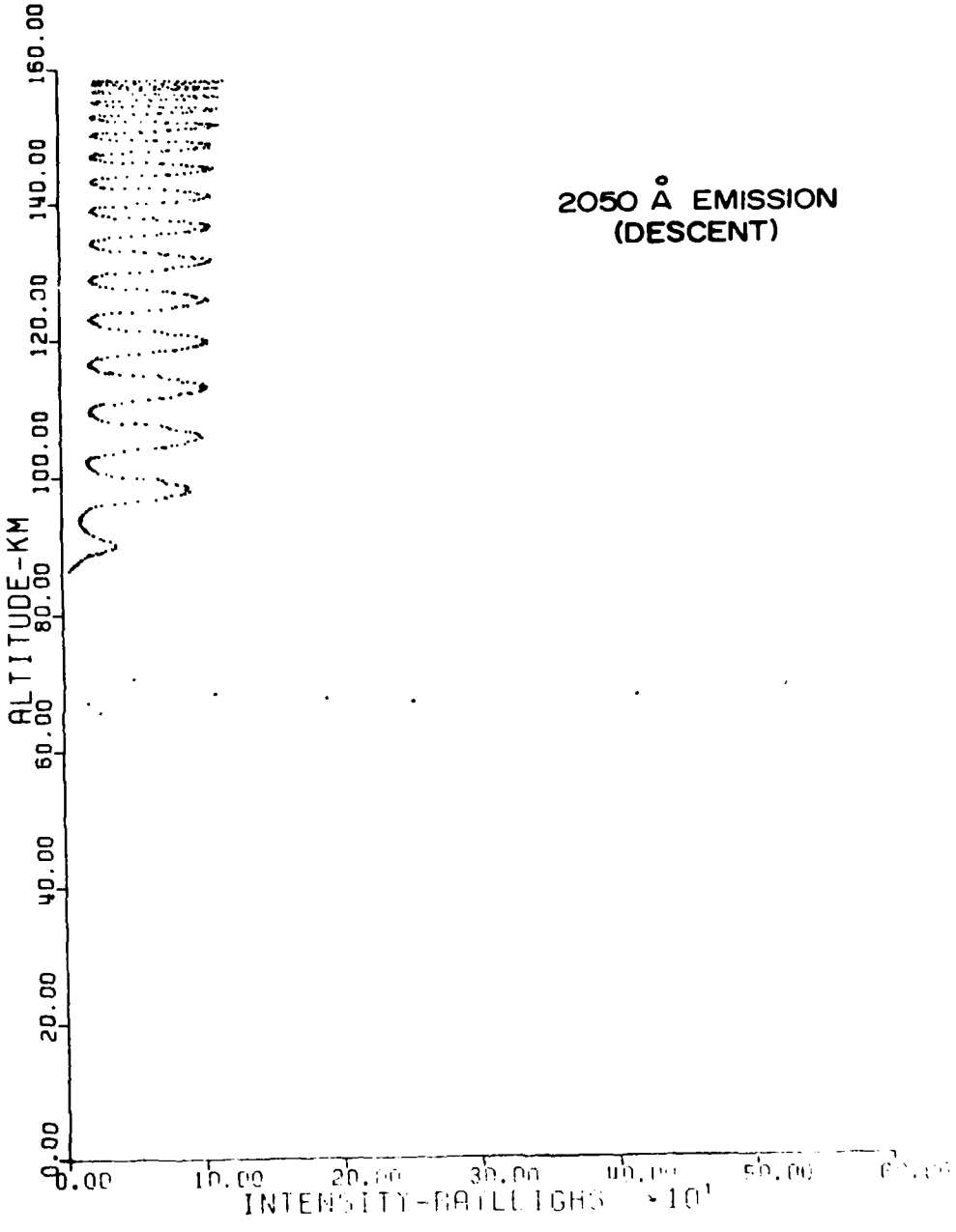

Figure 15. Descent profile of solar 2050A intensity. The modulation is due to vehicle precession and the solar disk being at the extreme edge of the detector field of view. Vehicle turnover was evidenced by the scattered high points at about 67 km.

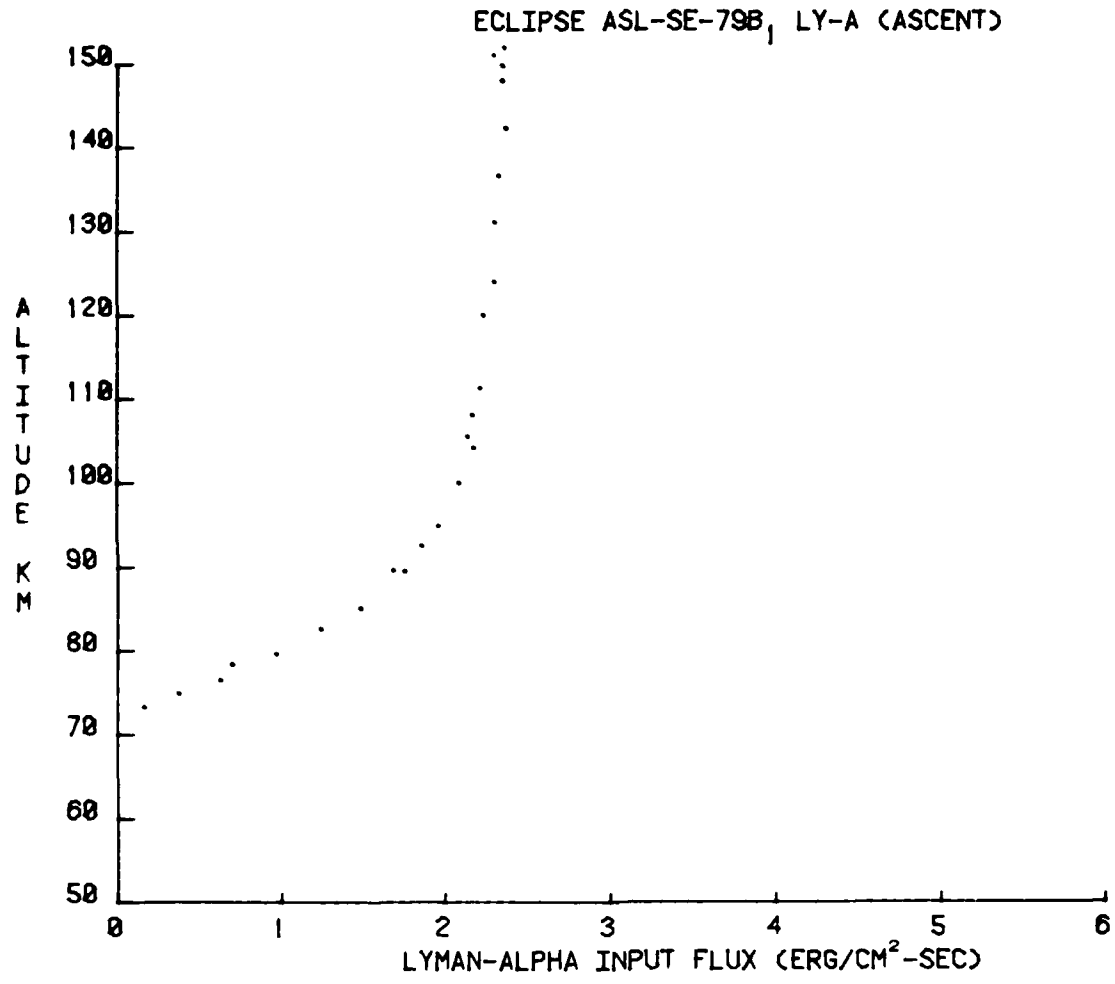

Figure 16. Ascent profile of Lyman-alpha radiance (B_1).

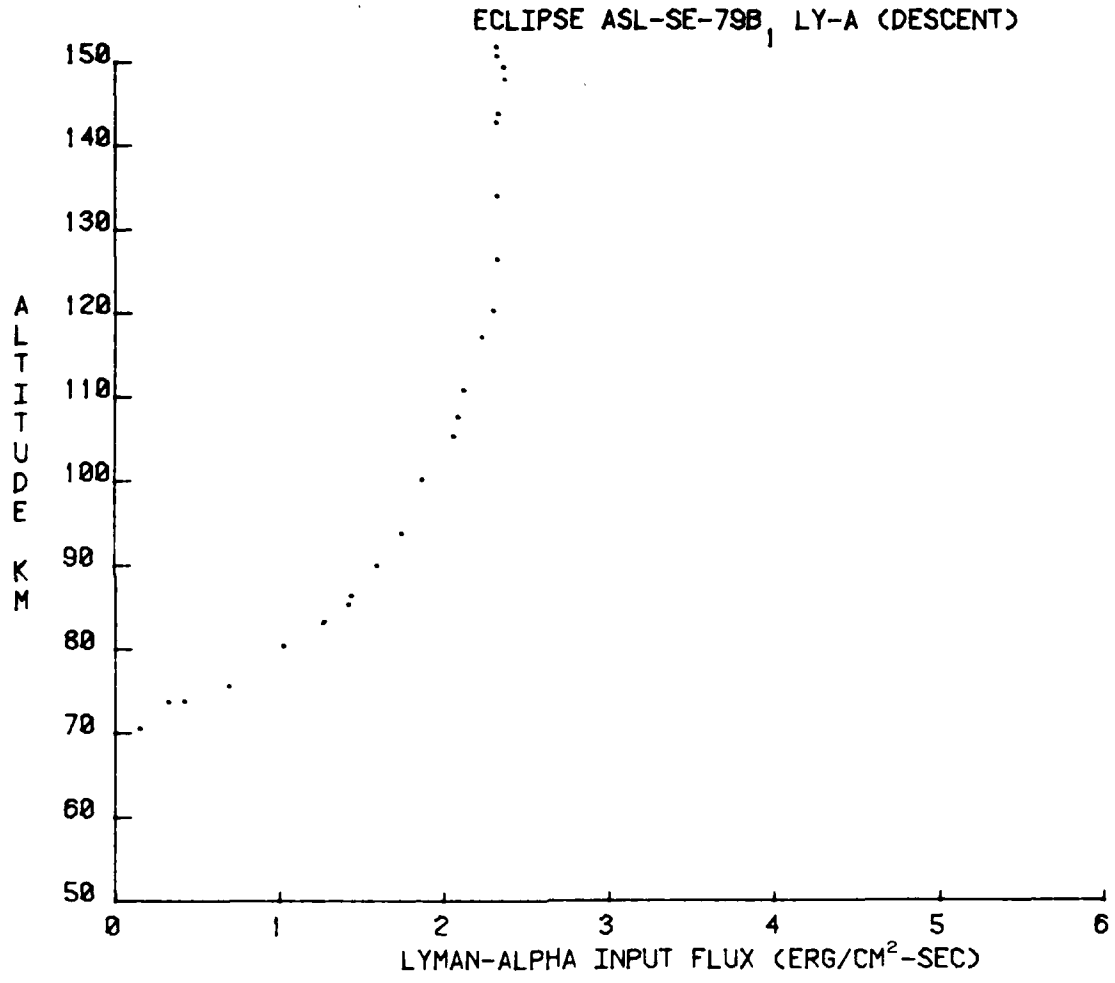

Figure 17. Descent profile of Lyman-alpha radiance (B_1).

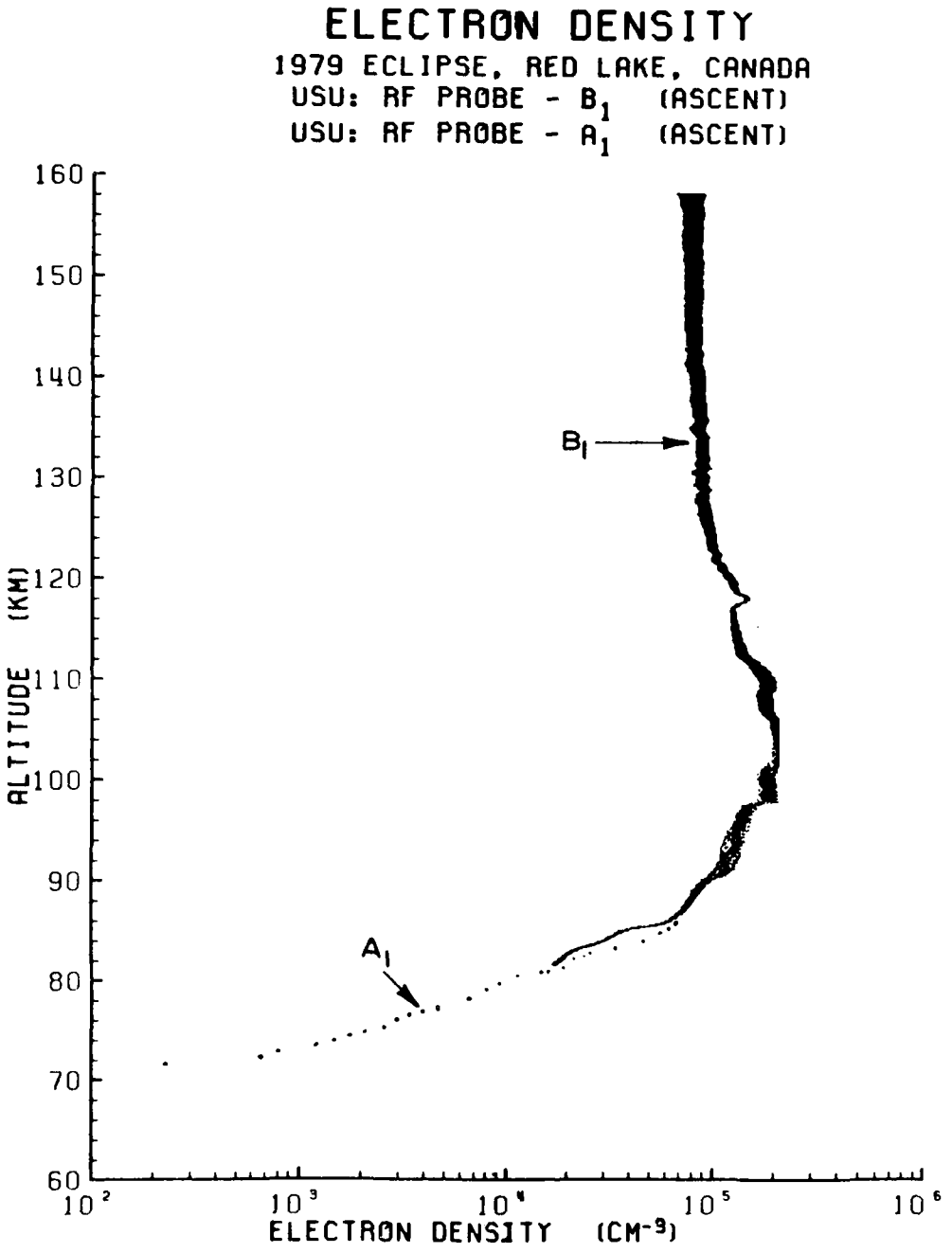

Figure 18. Composite electron density profile from ascent of rockets A_1 and B_1 derived from the RF admittance probe.

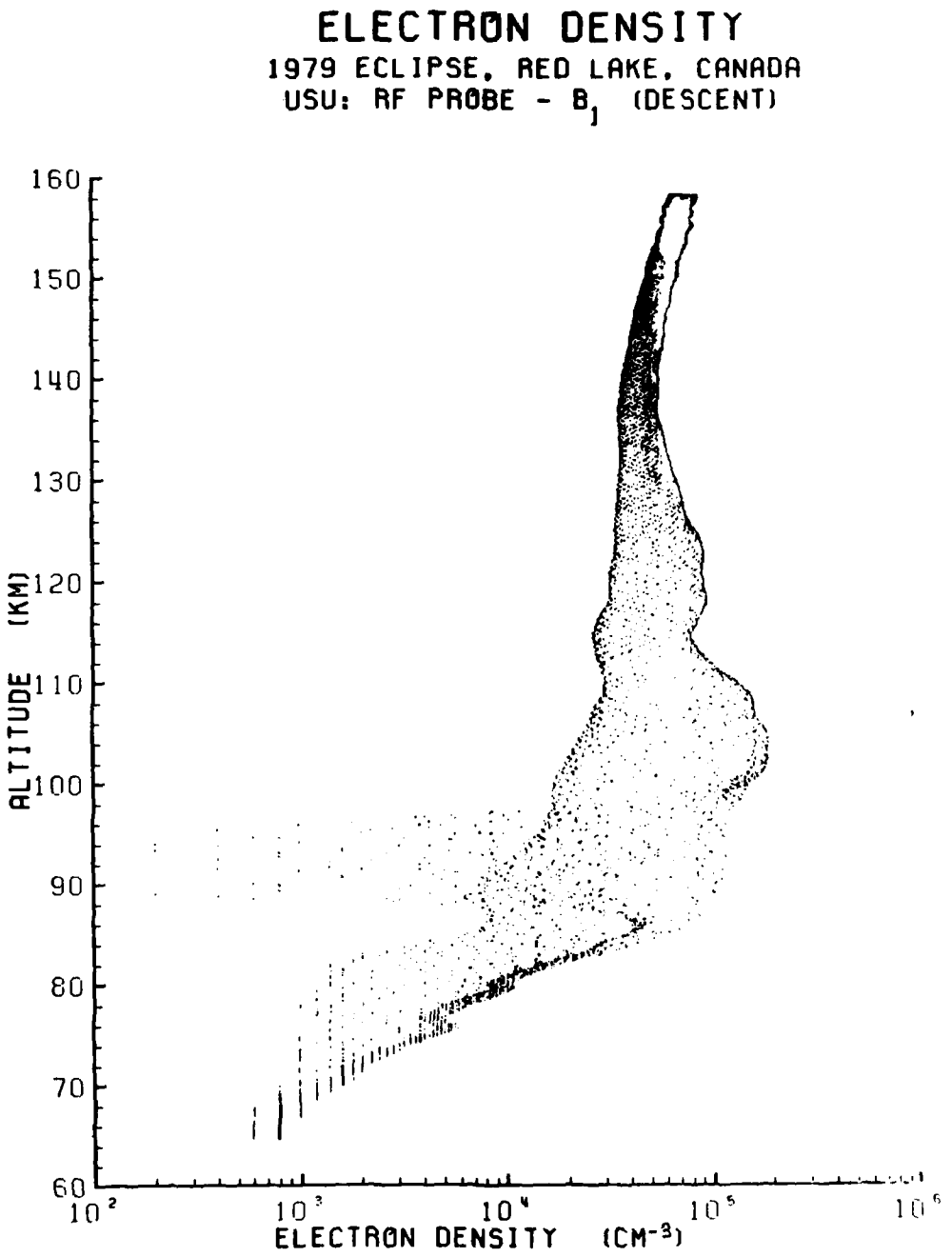

Figure 19. Descent electron density from RF probe on rocket B_1.

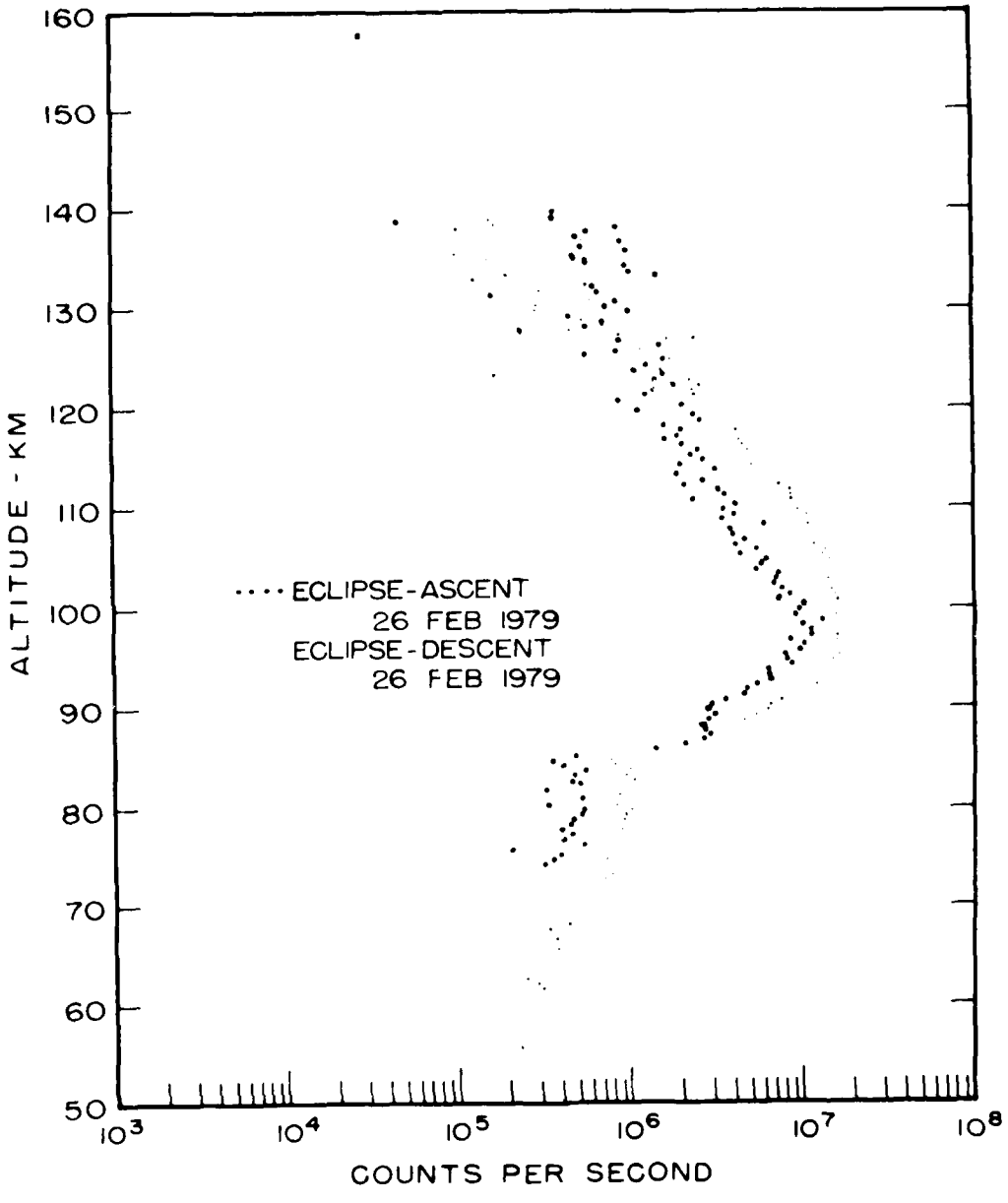

Figure 20. Atomic oxygen raw data profiles in terms of detector count rate vs altitude for both ascent and descent.

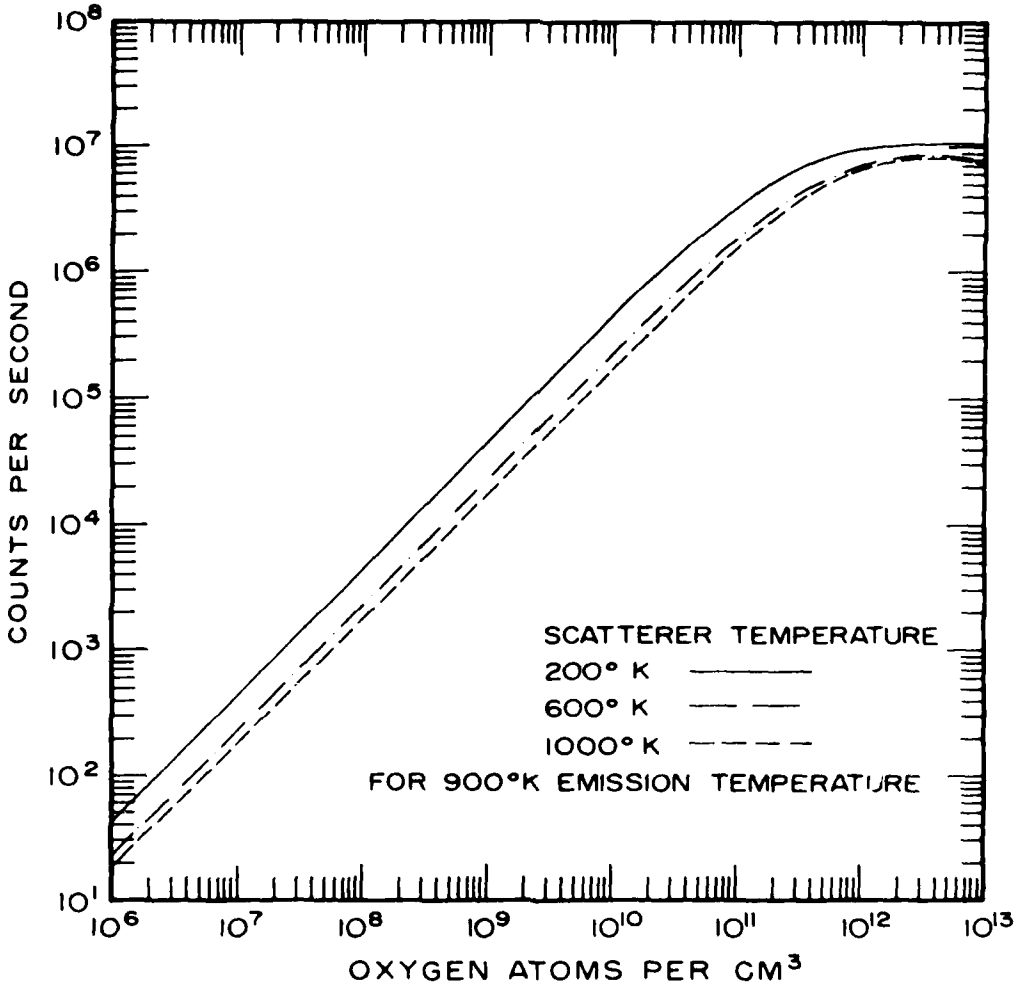

Figure 21. Response of resonant scattering system as flown during eclipse showing nonlinearity due to increasing optical depth at high O densities and sensitivity effects due to temperature.

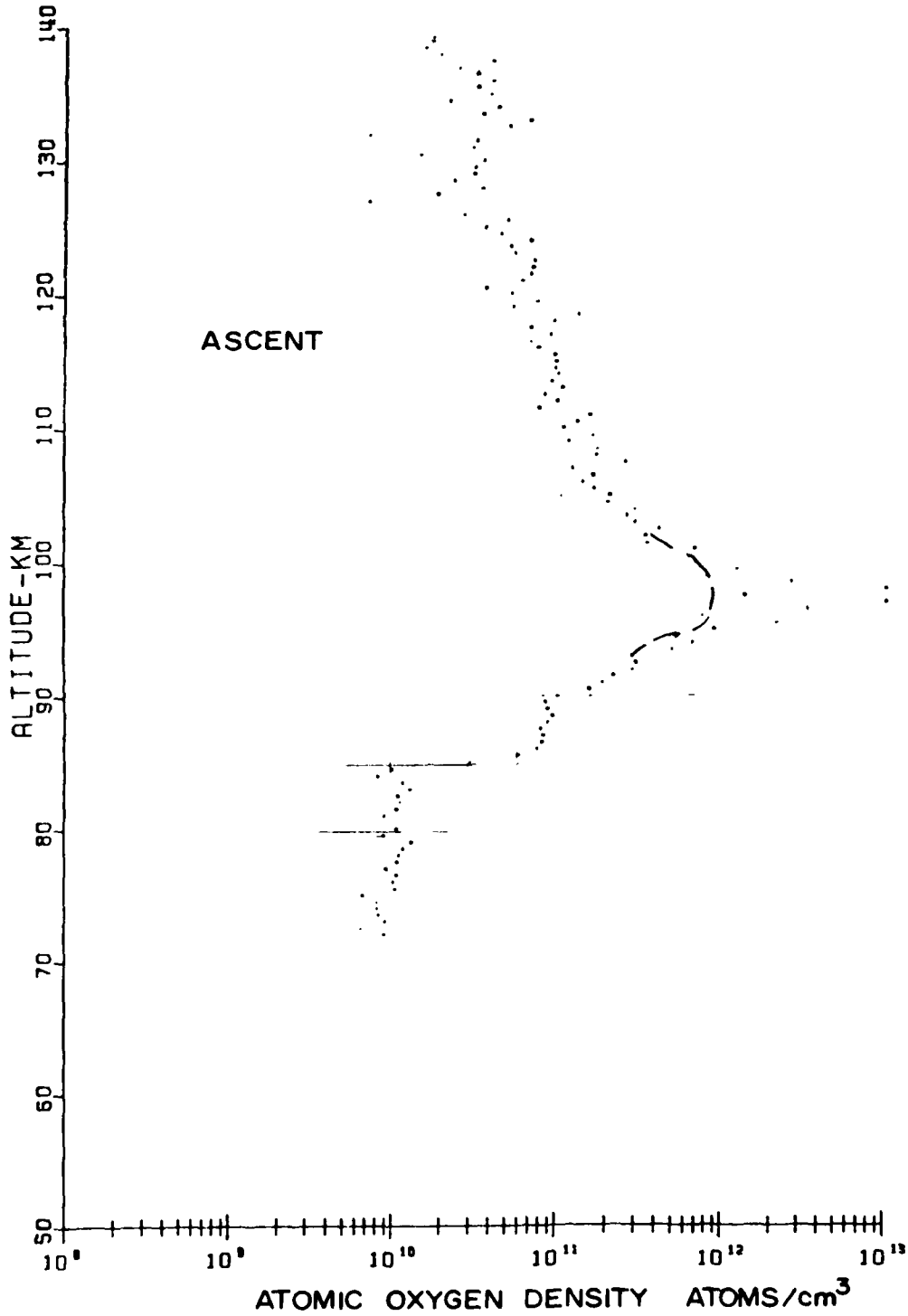

Figure 22. Measured ascent atomic oxygen profile.

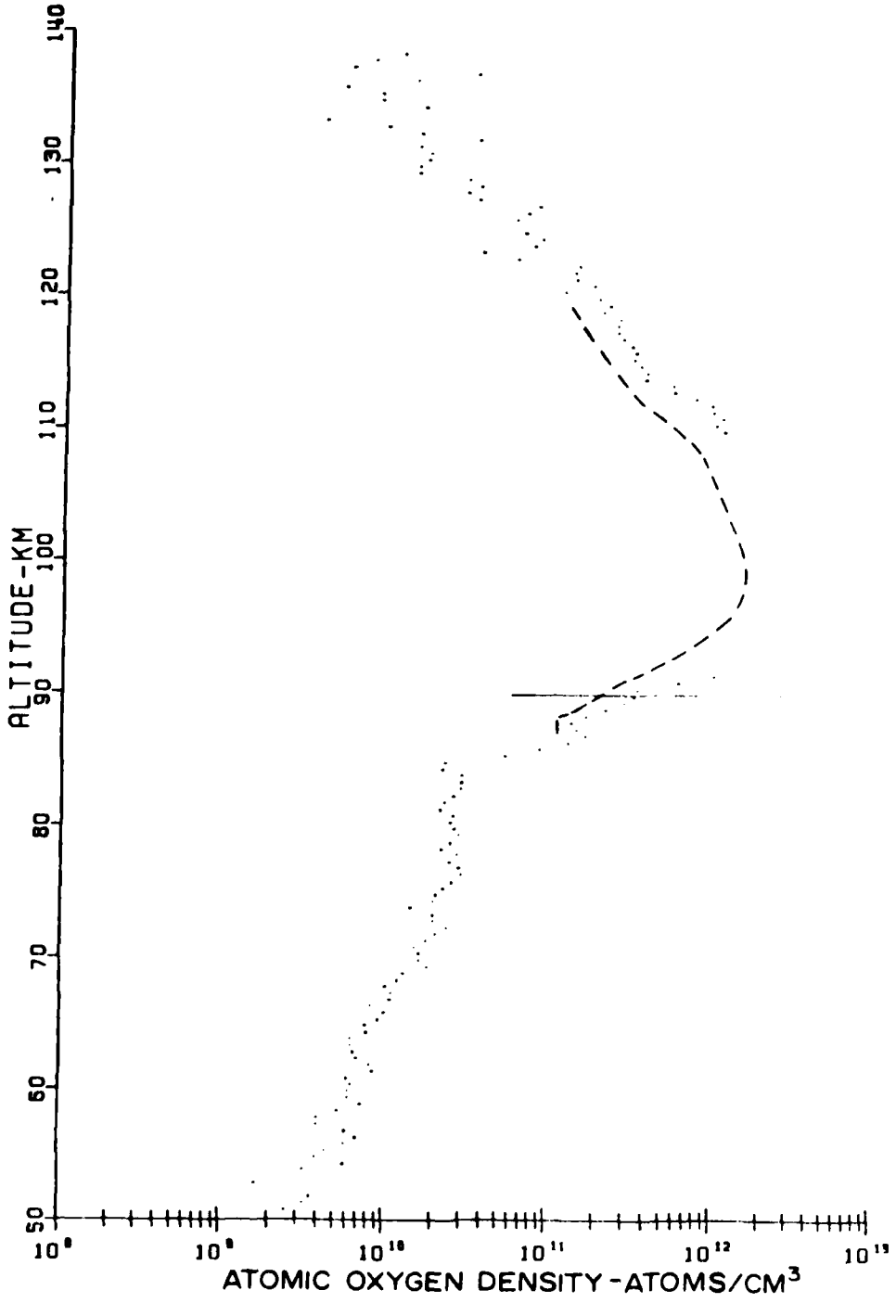

Figure 23. Measured descent atomic oxygen profile.

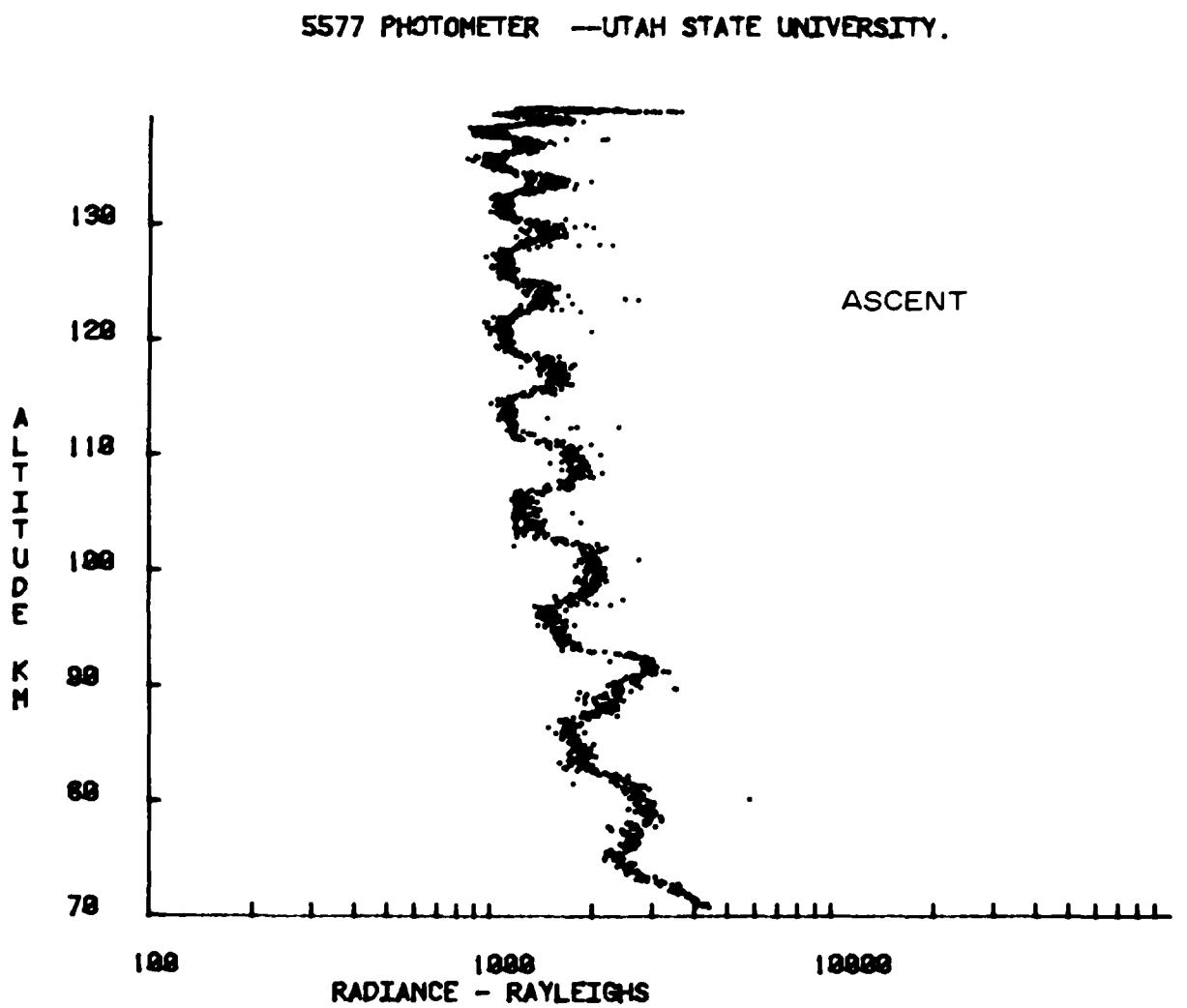

Figure 24. Measured 5577Å emission profile (ascent).

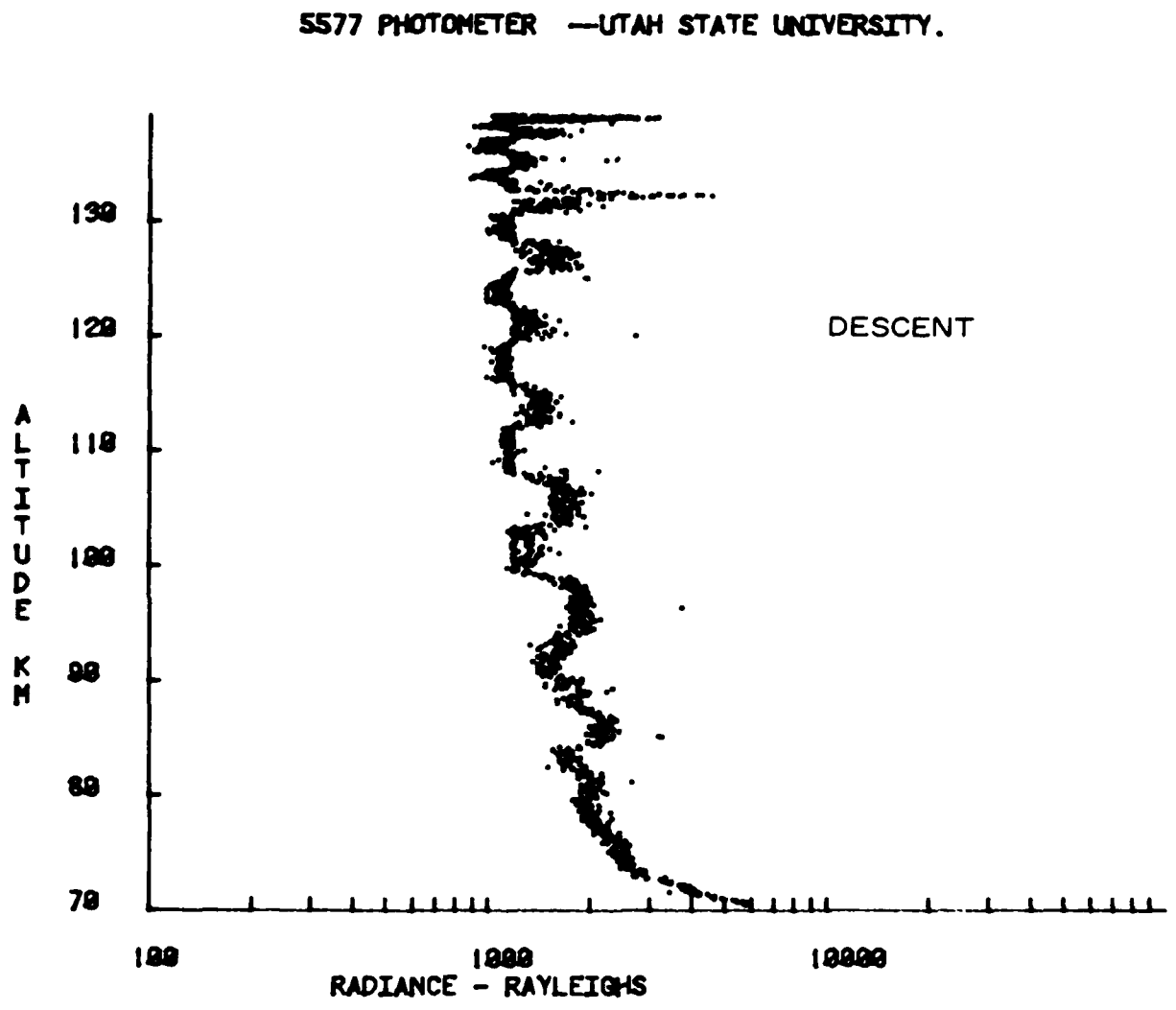

Figure 25. Measured 5577Å emission profile (descent).

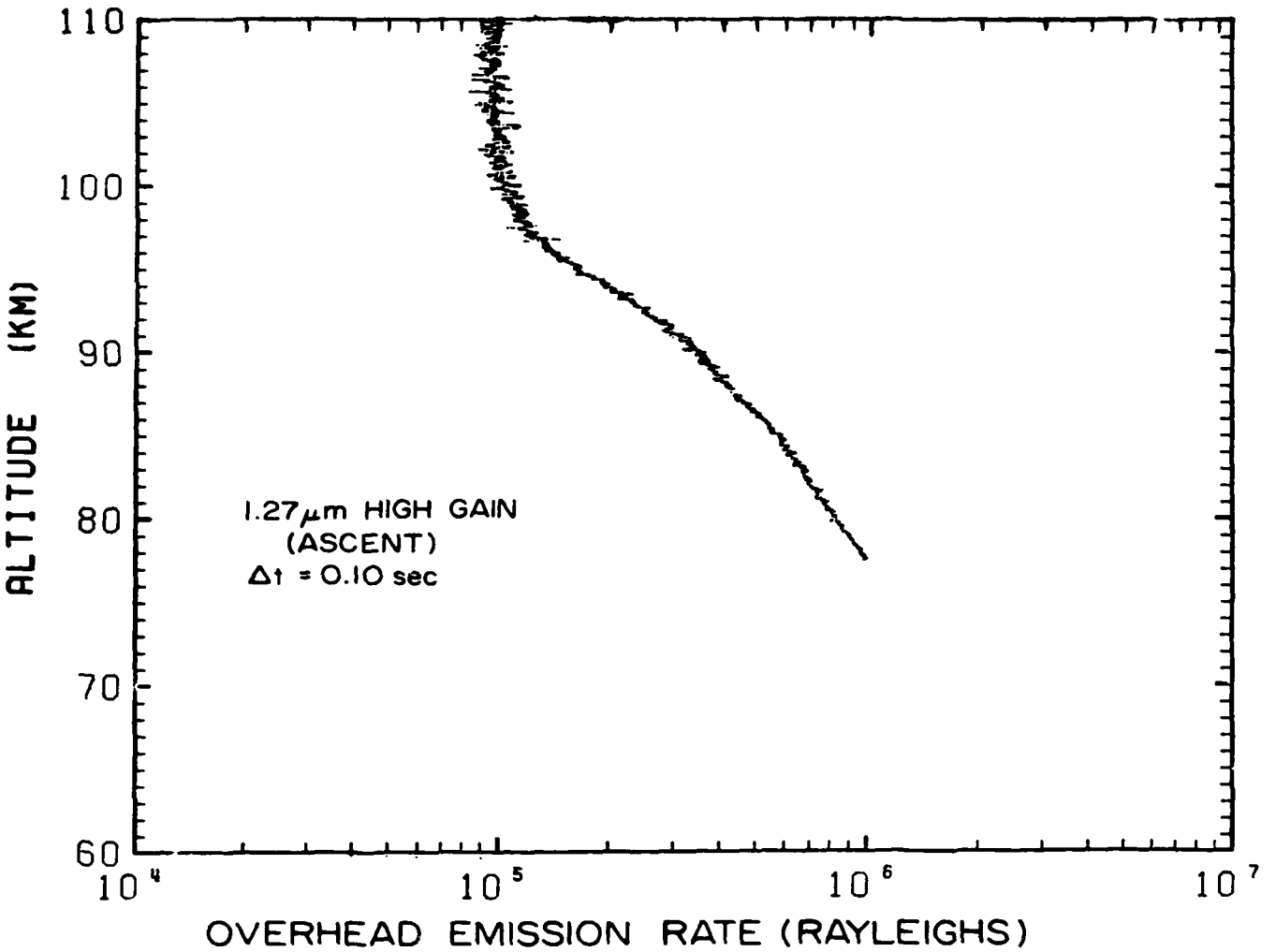

Figure 26. Overhead (column) emission rate at λ1.27μm based on ascent data from the high-gain channel. (A time constant of 0.10 s was used in smoothing the data.)

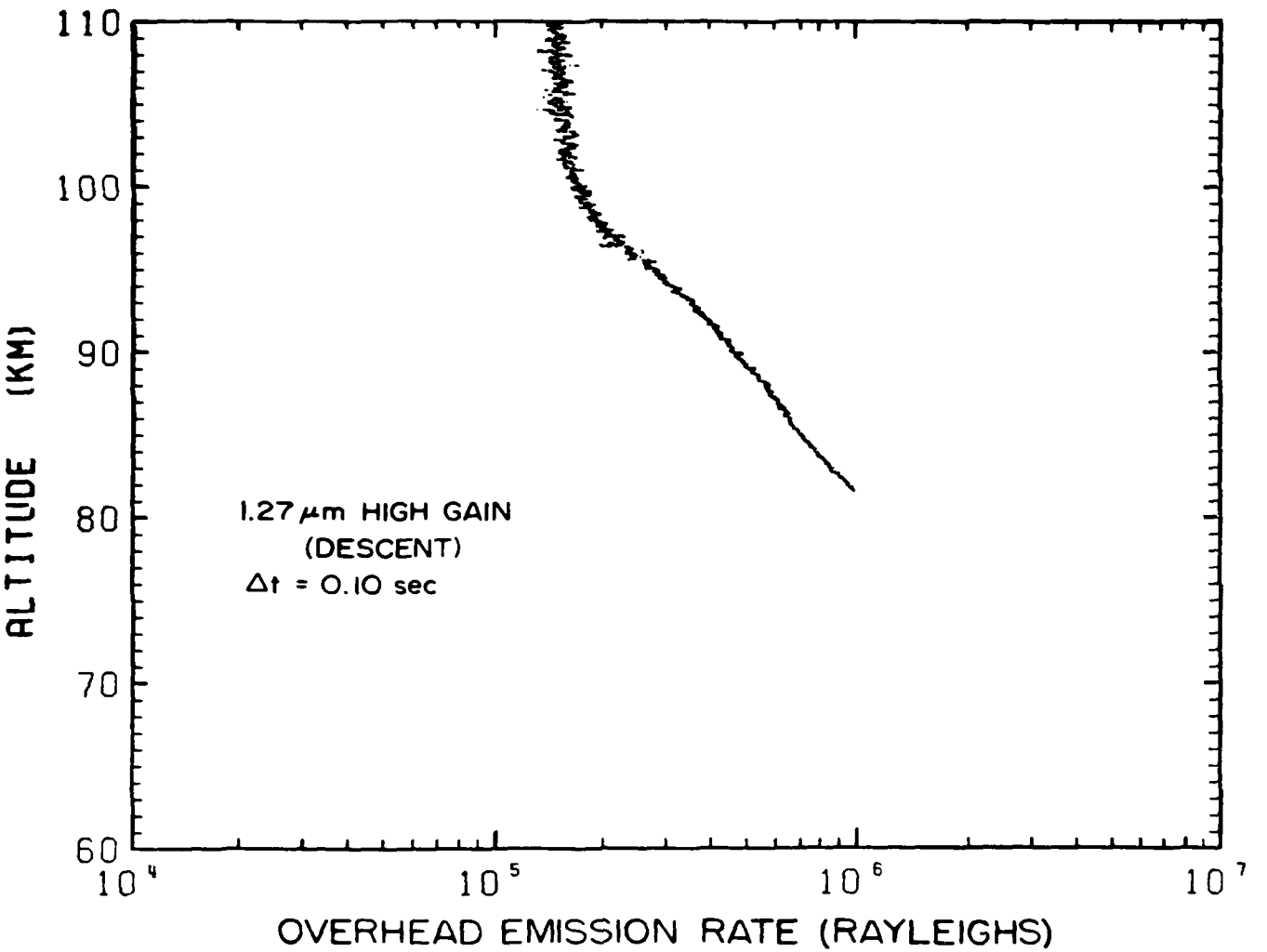

Figure 27. Overhead (column) emission rate at λ1.27μm based on descent data from the high-gain channel. (A time constant of 0.10 s was used in smoothing the data.)

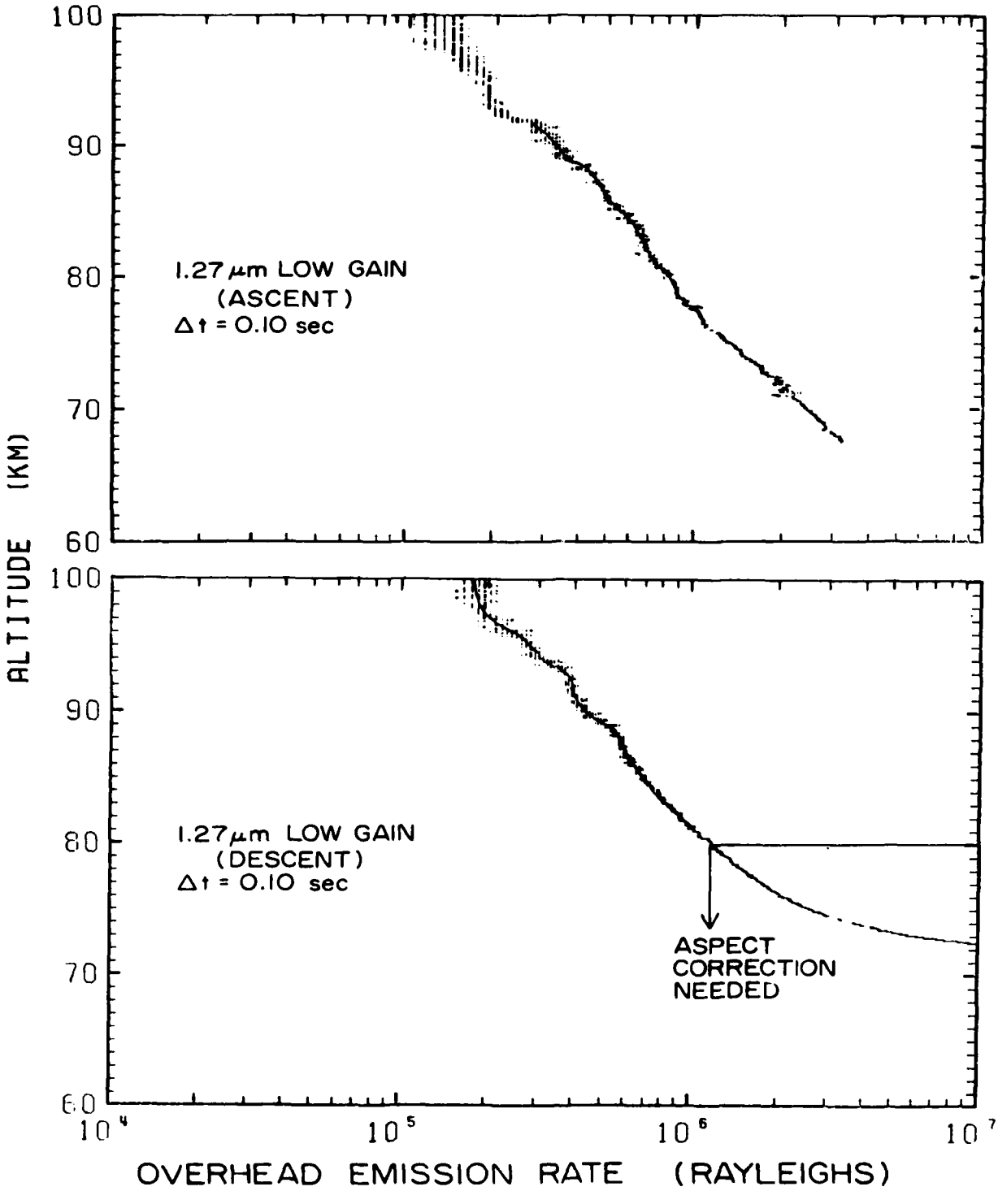

Figure 28. Overhead (column) emission rate at λ1.27μm based on ascent, descent data from the low-gain channel. (A time constant of 0.10 s was used in smoothing the data.)

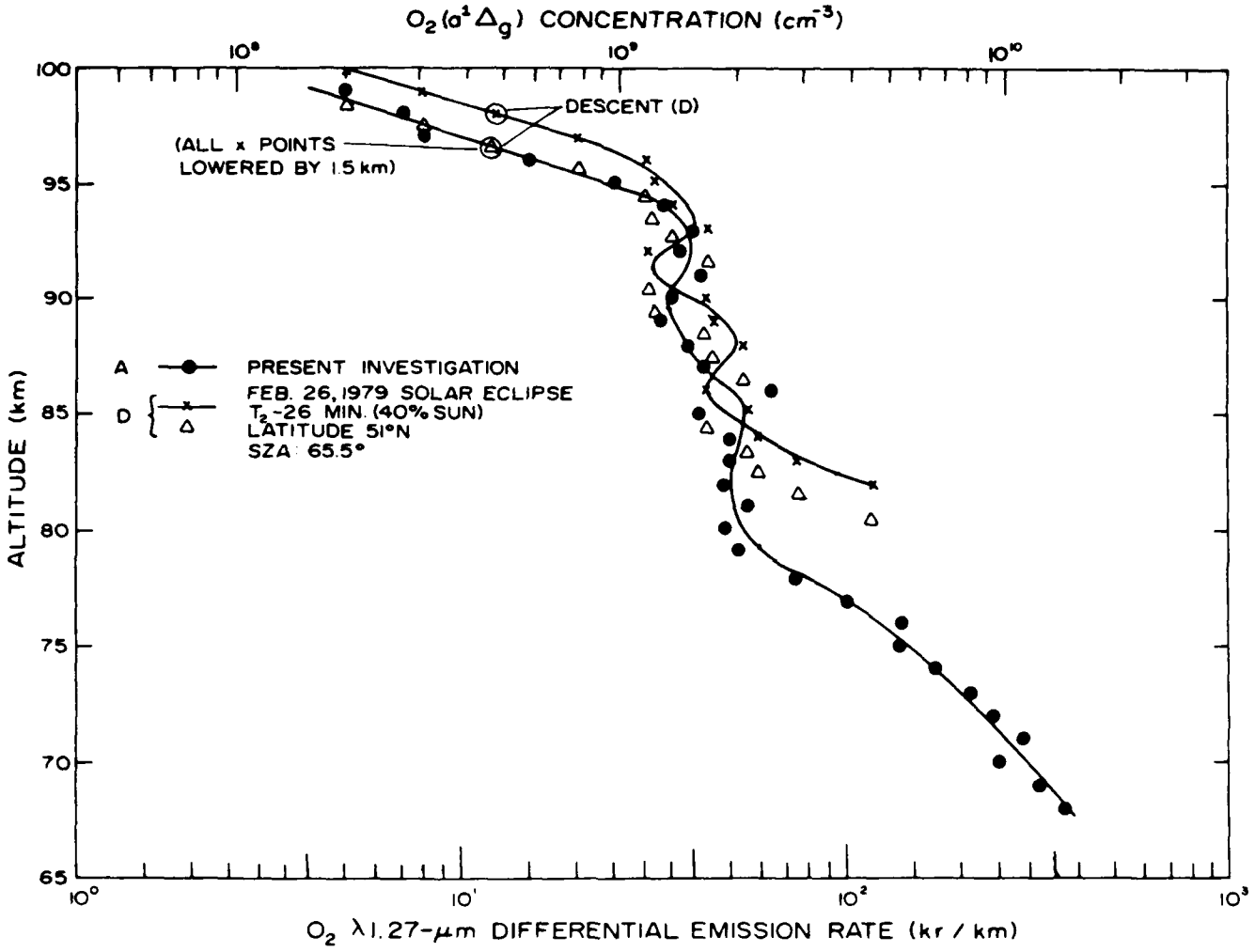

Figure 29. Differential emission rate and $O_2(a^1\Delta_g)$ profiles. (Note: the descent results below 86 km will require significant aspect corrections.)

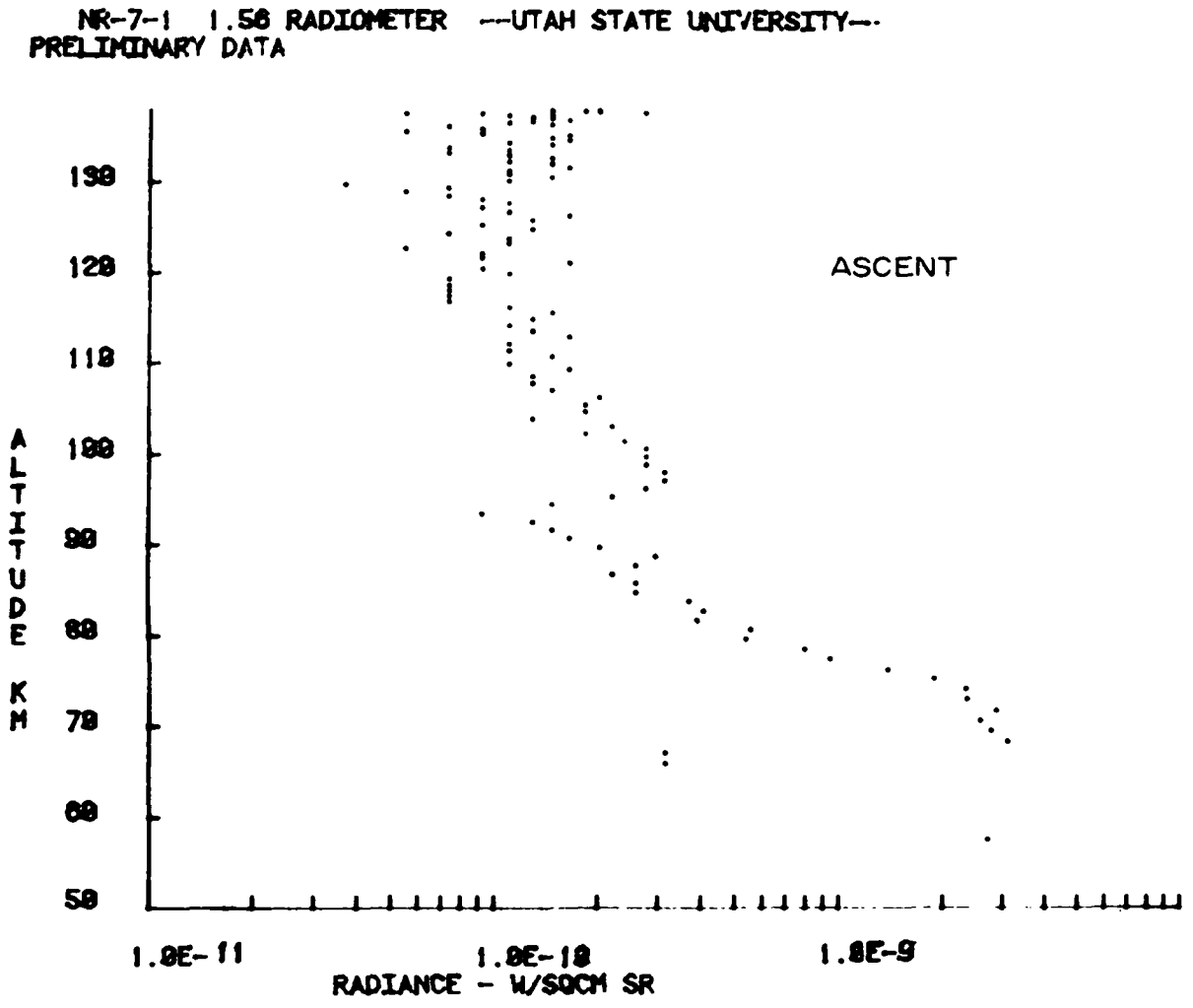

Figure 30. Overhead radiance profile from the $\lambda 1.56\mu m$ channel.

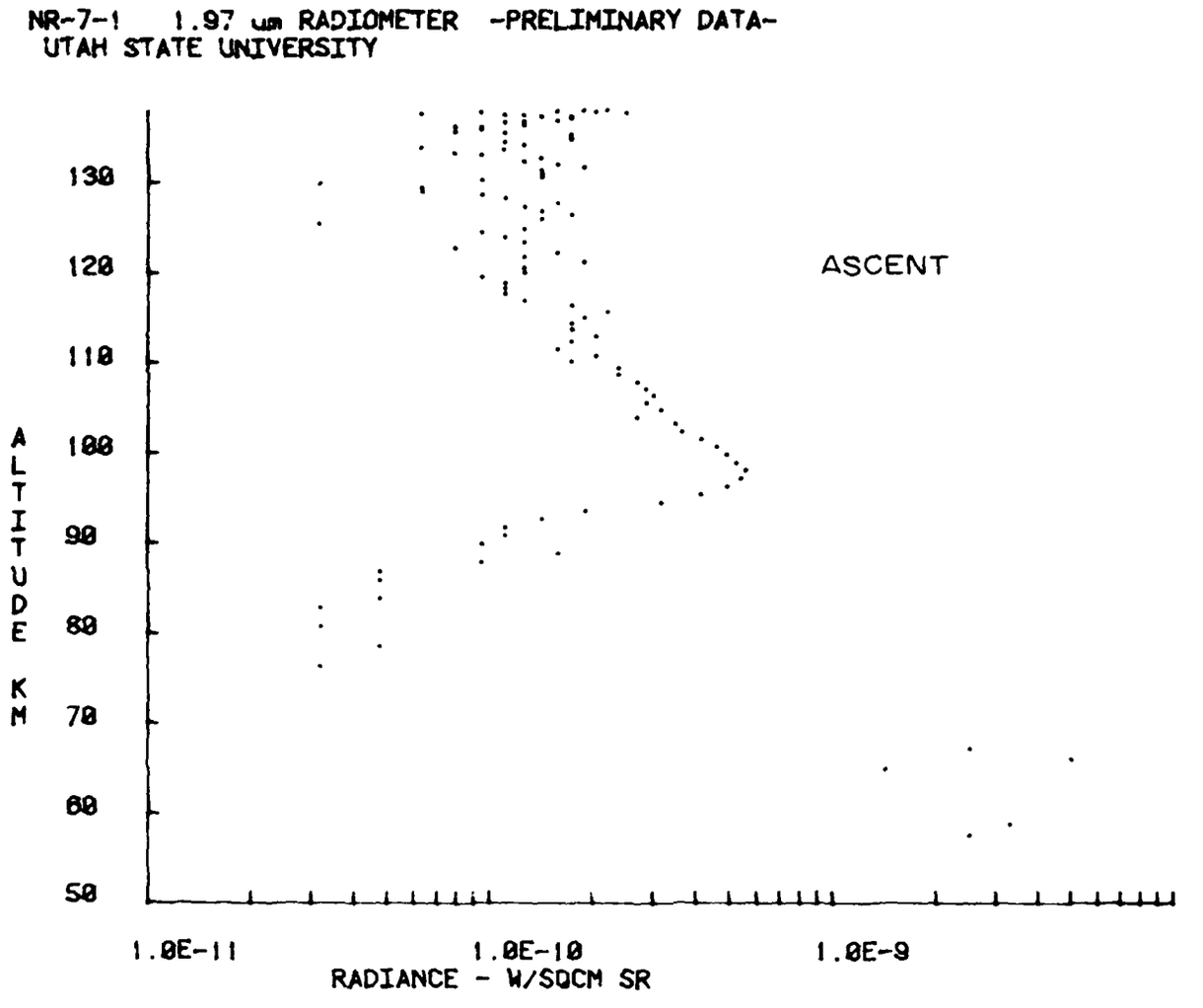

Figure 31. Overhead radiance profile from the λ1.97μm channel.

ELECTRO-OPTICS DISTRIBUTION LIST

Commander
US Army Aviation School
Fort Rucker, AL 36362

Commander
US Army Aviation Center
ATTN: ATZQ-D-MA (Mr. Oliver N. Heath)
Fort Rucker, AL 36362

Commander
US Army Aviation Center
ATTN: ATZQ-D-MS (Mr. Donald Wagner)
Fort Rucker, AL 36362

NASA/Marshall Space Flight Center
ATTN: ES-83 (Otha H. Vaughan, Jr.)
Huntsville, AL 35812

NASA/Marshall Space Flight Center
Atmospheric Sciences Division
ATTN: Code ES-81 (Dr. William W. Vaughan)
Huntsville, AL 35812

Nichols Research Corporation
ATTN: Dr. Lary W. Pinkley
4040 South Memorial Parkway
Huntsville, AL 35802

John M. Hobbie
c/o Kentron International
2003 Byrd Spring Road
Huntsville, AL 35802

Mr. Ray Baker
Lockheed-Missile & Space Company
4800 Bradford Blvd
Huntsville, AL 35807

Commander
US Army Missile Command
ATTN: DRSMI-OG (Mr. Donald R. Peterson)
Redstone Arsenal, AL 35809

Commander
US Army Missile Command
ATTN: DRSMI-OGA (Dr. Bruce W. Fowler)
Redstone Arsenal, AL 35809

Commander
US Army Missile Command
ATTN: DRSMI-REL (Dr. George Emmons)
Redstone Arsenal, AL 35809

Commander
US Army Missile Command
ATTN: DRSMI-REO (Huey F. Anderson)
Redstone Arsenal, AL 35809

Commander
US Army Missile Command
ATTN: DRSMI-REO (Mr. Maxwell W. Harper)
Redstone Arsenal, AL 35809

Commander
US Army Missile Command
ATTN: DRSMI-REO (Mr. Gene Widenhofer)
Redstone Arsenal, AL 35809

Commander
US Army Missile Command
ATTN: DRSMI-RHC (Dr. Julius Q. Lilly)
Redstone Arsenal, AL 35809

Commander
US Army Missile Command
Redstone Scientific Information Center
ATTN: DRSMI-RPRD (Documents Section)
Redstone Arsenal, AL 35809

Commander
US Army Missile Command
ATTN: DRSMI-RRA (Dr. Oskar Essenwanger)
Redstone Arsenal, AL 35809

Commander
US Army Missile Command
ATTN: DRSMI-RRO (Mr. Charles Christensen)
Redstone Arsenal, AL 35809

Commander
US Army Missile Command
ATTN: DRSMI-RRO (Dr. George A. Tanton)
Redstone Arsenal, AL 35809

Commander
US Army Communications Command
ATTN: CC-OPS-PP
Fort Huachuca, AZ 85613

Commander
US Army Intelligence Center & School
ATTN: ATSI-CD-CS (Mr. Richard G. Cundy)
Fort Huachuca, AZ 85613

Commander
US Army Intelligence Center & School
ATTN: ATSI-CD-MD (Mr. Harry Wilder)
Fort Huachuca, AZ 85613

Commander
US Army Intelligence Center & School
ATTN: ATSI-CS-C (2LT Coffman)
Fort Huachuca, AZ 85613

Commander
US Army Yuma Proving Ground
ATTN: STEYP-MSA-TL
Bldg 2105
Yuma, AZ 85364

Northrop Corporation
Electro-Mechanical Division
ATTN: Dr. Richard D. Tooley
500 East Orangethorpe Avenue
Anaheim, CA 92801

Commander
Naval Weapons Center
ATTN: Code 3918 (Dr. Alexis Shlanta)
China Lake, CA 93555

Hughes Helicopters
Army Advanced Attack Helicopter Weapons
ATTN: Mr. Charles R. Hill
Centinela and Teale Streets
Bldg 305, MS T-73A
Culter City, CA 90230

Commander
US Army Combat Developments
Experimentation Command
ATTN: ATEC-PL-M (Mr. Gary G. Love)
Fort Ord, CA 93941

SRI International
ATTN: K2060/Dr. Edward E. Uthe
333 Ravenswood Avenue
Menlo Park, CA 94025

SRI International
ATTN: Mr. J. E. Van der Laan
333 Ravenswood Avenue
Menlo Park, CA 94025

Joane May
Naval Environmental Prediction
Research Facility (NEPRF)
ATTN: Library
Monterey, CA 93940

Sylvania Systems Group,
Western Division
GTE Products Corporation
ATTN: Technical Reports Library
P.O. Box 205
Mountain View, CA 94042

Sylvania Systems Group
Western Division
GTE Products Corporation
ATTN: Mr. Lee W. Carrier
P.O. Box 188
Mountain View, CA 94042

Pacific Missile Test Center
Geophysics Division
ATTN: Code 3253
Point Mugu, CA 93042

Pacific Missile Test Center
Geophysics Division
ATTN: Code 3253 (Terry E. Battalino)
Point Mugu, CA 93042

Effects Technology Inc.
ATTN: Mr. John D. Carlyle
5383 Hollister Avenue
Santa Barbara, CA 93111

Commander
Naval Ocean Systems Center
ATTN: Code 532 (Dr. Juergen Richter)
San Diego, CA 92152

Commander
Naval Ocean Systems Center
ATTN: Code 5322 (Mr. Herbert G. Hughes)
San Diego, CA 92152

Commander
Naval Ocean Systems Center
ATTN: Code 4473 (Tech Library)
San Diego, CA 92152

The RAND Corporation
ATTN: Ralph Huschke
1700 Main Street
Santa Monica, CA 90406

Particle Measuring Systems, Inc.
ATTN: Dr. Robert G. Knollenberg
1855 South 57th Court
Boulder, CO 80301

US Department of Commerce
National Oceanic and Atmospheric Admin
Environmental Research Laboratories
ATTN: Library, R-51, Technical Reports
325 Broadway
Boulder, CO 80303

US Department of Commerce
National Oceanic and Atmospheric Admin
Environmental Research Laboratories
ATTN: R45X3 (Dr. Vernon E. Derr)
Boulder, CO 80303

US Department of Commerce
National Telecommunications and
Information Administration
Institute for Telecommunication Sciences
ATTN: Code 1-3426 (Dr. Hans J. Liebe)
Boulder, CO 80303

AFATL/DLODL
Technical Library
Eglin AFB, FL 32542

Commanding Officer
Naval Training Equipment Center
ATTN: Technical Information Center
Orlando, FL 32813

Georgia Institute of Technology
Engineering Experiment Station
ATTN: Dr. Robert W. McMillan
Atlanta, GA 30332

Georgia Institute of Technology
Engineering Experiment Station
ATTN: Dr. James C. Wiltse
Atlanta, GA 30332

Commandant
US Army Infantry Center
ATTN: ATSH-CD-MS-E (Mr. Robert McKenna)
Fort Benning, GA 31805

Commander
US Army Signal Center & Fort Gordon
ATTN: ATZHCD-CS
Fort Gordon, GA 30905

Commander
US Army Signal Center & Fort Gordon
ATTN: ATZHCD-O
Fort Gordon, GA 30905

USAFETAC/DNE
ATTN: Mr. Charles Glauber
Scott AFB, IL 62225

Commander
Air Weather Service
ATTN: AWS/DNDP (LTC Kit G. Cottrell)
Scott AFB, IL 62225

Commander
Air Weather Service
ATTN: AWS/DOOF (MAJ Robert Wright)
Scott AFB, IL 62225

Commander
US Army Combined Arms Center
& Ft. Leavenworth
ATTN: ATZLCA-CAA-Q (Mr. H. Kent Pickett)
Fort Leavenworth, KS 66027

Commander
US Army Combined Arms Center
& Ft. Leavenworth
ATTN: ATZLCA-SAN (Robert DeKinder, Jr.)
Fort Leavenworth, KS 66027

Commander
US Army Combined Arms Center
& Ft. Leavenworth
ATTN: ATZLCA-SAN (Mr. Kent I. Johnson)
Fort Leavenworth, KS 66027

Commander
US Army Combined Arms Center
& Ft. Leavenworth
ATTN: ATZLCA-WE (LTC Darrell Holland)
Fort Leavenworth, KS 66027

President
USAARENBD
ATTN: ATZK-AE-TA (Dr. Charles R. Leake)
Fort Knox, KY 40121

Commander
US Army Armor Center and Fort Knox
ATTN: ATZK-CD-MS
Fort Knox, KY 40121

Commander
US Army Armor Center and Fort Knox
ATTN: ATZK-CD-SD
Fort Knox, KY 40121

Aerodyne Research Inc.
ATTN: Dr. John F. Ebersole
Crosby Drive
Bedford, MA 01730

Commander
Air Force Geophysics Laboratory
ATTN: OPA (Dr. Robert W. Fenn)
Hanscom AFB, MA 01731

Commander
Air Force Geophysics Laboratory
ATTN: OPI (Dr. Robert A. McClatchey)
Hanscom AFB, MA 01731

Massachusetts Institute of Technology
Lincoln Laboratory
ATTN: Dr. T. J. Goblick, B-370
P.O. Box 73
Lexington, MA 02173

Massachusetts Institute of Technology
Lincoln Laboratory
ATTN: Dr. Michael Gruber
P.O. Box 73
Lexington, MA 02173

Raytheon Company
Equipment Division
ATTN: Dr. Charles M. Sonnenschein
430 Boston Post Road
Wayland, MA 01778

Commander
US Army Ballistic Research Laboratory/
ARRADCOM
ATTN: DRDAR-BLB (Mr. Richard McGee)
Aberdeen Proving Ground, MD 21005

Commander/Director
Chemical Systems Laboratory
US Army Armament Research
& Development Command
ATTN: DRDAR-CLB-PS (Dr. Edward Stuebing)
Aberdeen Proving Ground, MD 21010

Commander/Director
Chemical Systems Laboratory
US Army Armament Research
& Development Command
ATTN: DRDAR-CLB-PS (Mr. Joseph Vervier)
Aberdeen Proving Ground, MD 21010

Commander/Director
Chemical Systems Laboratory
US Army Armament Research
& Development Command
ATTN: DRDAR-CLY-A (Mr. Ronnald Pennsyle)
Aberdeen Proving Ground, MD 21010

Commander
US Army Ballistic Research Laboratory/
ARRADCOM
ATTN: DRDAR-TSB-S (STINFO)
Aberdeen Proving Ground, MD 21005

Commander
US Army Electronics Research
& Development Command
ATTN: DRDEL-CCM (W. H. Pepper)
Adelphi, MD 20783

Commander
US Army Electronics Research
& Development Command
ATTN: DRDEL-CG/DRDEL-DC/DRDEL-CS
2800 Powder Mill Road
Adelphi, MD 20783

Commander
US Army Electronics Research
& Development Command
ATTN: DRDEL-CT
2800 Powder Mill Road
Adelphi, MD 20783

Commander
US Army Electronics Research
& Development Command
ATTN: DRDEL-PAO (Mr. Steven Kimmel)
2800 Powder Mill Road
Adelphi, MD 20783

Project Manager
Smoke/Obscurants
ATTN: DRDPM-SMK
(Dr. Anthony Van de Wal, Jr.)
Aberdeen Proving Ground, MD 21005

Project Manager
Smoke/Obscurants
ATTN: DRDPM-SMK-T (Mr. Sidney Gerard)
Aberdeen Proving Ground, MD 21005

Commander
US Army Test & Evaluation Command
ATTN: DRSTE-AD-M (Mr. Warren M. Baity)
Aberdeen Proving Ground, MD 21005

Commander
US Army Test & Evaluation Command
ATTN: DRSTE-AD-M (Dr. Norman E. Pentz)
Aberdeen Proving Ground, MD 21005

Director
US Army Materiel Systems Analysis Activity
ATTN: DRXSY-AAM (Mr. William Smith)
Aberdeen Proving Ground, MD 21005

Director
US Army Materiel Systems Analysis Activity
ATTN: DRXSY-CS (Mr. Philip H. Beavers)
Aberdeen Proving Ground, MD 21005

Director
US Army Materiel Systems Analysis Activity
ATTN: DRXSY-GB (Wilbur L. Warfield)
Aberdeen Proving Ground, MD 21005

Director
US Army Materiel Systems Analysis Activity
ATTN: DRXSY-GP (Mr. Fred Campbell)
Aberdeen Proving Ground, MD 21005

Director
US Army Materiel Systems Analysis Activity
ATTN: DRXSY-GS
(Mr. Michael Starks/Mr. Julian Chernick)
Aberdeen Proving Ground, MD 21005

Director
US Army Materiel Systems Analysis Activity
ATTN: DRXSY-J (Mr James F. O'Bryon)
Aberdeen Proving Ground, MD 21005

Director
US Army Materiel Systems Analysis Activity
ATTN: DRXSY-LM (Mr. Robert M. Marchetti)
Aberdeen Proving Ground, MD 21005

Commander
Harry Diamond Laboratories
ATTN: Dr. William W. Carter
2800 Powder Mill Road
Adelphi, MD 20783

Commander
Harry Diamond Laboratories
ATTN: DELHD-R-CM (Mr. Robert McCoskey)
2800 Powder Mill Road
Adelphi, MD 20783

Commander
Harry Diamond Laboratories
ATTN: DELHD-R-CM-NM (Dr. Robert Humphrey)
2800 Powder Mill Road
Adelphi, MD 20783

Commander
Harry Diamond Laboratories
ATTN: DELHD-R-CM-NM (Dr. Z. G. Sztankay)
2800 Powder Mill Road
Adelphi, MD 20783

Commander
Harry Diamond Laboratories
ATTN: DELHD-R-CM-NM (Dr. Joseph Nemarich)
2800 Powder Mill Road
Adelphi, MD 20783

Commander
Air Force Systems Command
ATTN: WER (Mr. Richard F. Picanso)
Andrews AFB, MD 20334

Martin Marietta Laboratories
ATTN: Jar Mo Chen
1450 South Rolling Road
Baltimore, MD 21227

Commander
US Army Concepts Analysis Agency
ATTN: CSCA-SMC (Mr. Hal E. Hock)
8120 Woodmont Avenue
Bethesda, MD 20014

Director
National Security Agency
ATTN: R52/Dr. Douglas Woods
Fort George G. Meade, MD 20755

Chief
Intelligence Materiel Development
& Support Office
US Army Electronic Warfare Laboratory
ATTN: DELEW-I (LTC Kenneth E. Thomas)
Fort George G. Meade, MD 20755

The John Hopkins University
Applied Physics Laboratory
ATTN: Dr. Michael J. Lun
John Hopkins Road
Laurell, MD 20810

Dr. Stephen T. Hanley
1720 Rhodesia Avenue
Oxon Hill, MD 20022

Science Applications Inc.
ATTN: Mr. G. D. Currie
15 Research Drive
Ann Arbor, MI 48103

Science Applications Inc.
ATTN: Dr. Robert E. Turner
15 Research Drive
Ann Arbor, MI 48103

Commander
US Army Tank-Automotive Research
& Development Command
ATTN: DRDTA-ZSC (Mr. Harry Young)
Warren, MI 48090

Commander
US Army Tank Automotive Research
& Development Command
ATTN: DRDTA-ZSC (Mr. Wallace Mick, Jr.)
Warren, MI 48090

Dr. A. D. Belmont
Research Division
Control Data Corporation
P.O. Box 1249
Minneapolis, MN 55440

Director
US Army Engr Waterways Experiment Station
ATTN: WESEN (Mr. James Mason)
P.O. Box 631
Vicksburg, MS 39180

Commander
US Army Research Office
ATTN: DRXRO-GS (Dr. Leo Alpert)
P.O. Box 12211
Research Triangle Park, NC 27709

Commander
US Army Research Office
ATTN: DRXRO-PP (Brenda Mann)
P.O. Box 12211
Research Triangle Park, NC 27709

Commander
US Army Cold Regions Research
& Engineering Laboratory
ATTN: CRREL-RD (Dr. K. F. Sterrett)
Hanover, NH 03755

Commander/Director
US Army Cold Regions Research
& Engineering Laboratory
ATTN: CRREL-RG (Mr. George Aitken)
Hanover, NH 03755

Commander
US Army Cold Regions Research
& Engineering Laboratory
ATTN: CRREL-RG (Mr. Roger H. Berger)
Hanover, NH 03755

Commander
US Army Armament Research
& Development Command
ATTN: DRDAR-AC (Mr. James Greenfield)
Dover, NJ 07801

Commander
US Army Armament Research
& Development Command
ATTN: DRDAR-TSS (Bldg #59)
Dover, NJ 07801

Commander
US Army Armament Research
& Development Command
ATTN: DRCPM-CAWS-EI (Mr. Peteris Jansons)
Dover, NJ 07801

Commander
US Army Armament Research
& Development Command
ATTN: DRCPM-CAWS-EI (Mr. G. H. Waldron)
Dover, NJ 07801

Deputy Joint Project Manager
for Navy/USMC SAL GP
ATTN: DRCPM-CAWS-NV (CPT Joseph Miceli)
Dover, NJ 07801

Commander/Director
US Army Combat Surveillance & Target
Acquisition Laboratory
ATTN: DELCS-I (Mr. David Longinotti)
Fort Monmouth, NJ 07703

Commander/Director
US Army Combat Surveillance & Target
Acquisition Laboratory
ATTN: DELCS-PE (Mr. Ben A. Di Campli)
Fort Monmouth, NJ 07703

Commander/Director
US Army Combat Surveillance & Target
Acquisition Laboratory
ATTN: DELCS-R-S (Mr. Donald L. Foiani)
Fort Monmouth, NJ 07703

Director
US Army Electronics Technology &
Devices Laboratory
ATTN: DELET-DD (S. Danko)
Fort Monmouth, NJ 07703

Project Manager
FIREFINDER/REMBASS
ATTN: DRCPM-FFR-TM (Mr. John M. Bialo)
Fort Monmouth, NJ 07703

Commander
US Army Electronics Research
& Development Command
ATTN: DRDEL-SA (Dr. Walter S. McAfee)
Fort Monmouth, NJ 07703

OLA, 2WS (MAC)
Holloman AFB, NM 88330

Commander
Air Force Weapons Laboratory
ATTN: AFWL/WE (MAJ John R. Elrick)
Kirtland, AFB, NM 87117

Director
USA TRADOC Systems Analysis Activity
ATTN: ATAA-SL
White Sands Missile Range, NM 88002

Director
USA TRADOC Systems Analysis Activity
ATTN: ATAA-SL (Dolores Anguiano)
White Sands Missile Range, NM 88002

Director
USA TRADOC Systems Analysis Activity
ATTN: ATAA-TDB (Mr. Louie Dominguez)
White Sands Missile Range, NM 88002

Director
USA TRADOC Systems Analysis Activity
ATTN: ATAA-TDB (Mr. William J. Leach)
White Sands Missile Range, NM 88002

Director
USA TRADOC Systems Analysis Activity
ATTN: ATAA-TGP (Mr. Roger F. Willis)
White Sands Missile Range, NM 88002

Director
Office of Missile Electronic Warfare
ATTN: DELEW-M-STO (Dr. Steven Kovel)
White Sands Missile Range, NM 88002

Office of the Test Director
Joint Services EO GW CM Test Program
ATTN: DRXDE-TD (Mr. Weldon Findley)
White Sands Missile Range, NM 88002

Commander
US Army White Sands Missile Range
ATTN: STEWS-PT-AL (Laurel B. Saunders)
White Sands Missile Range, NM 88002

Commander
US Army R&D Coordinator
US Embassy - Bonn
Box 165
APO New York 09080

Grumman Aerospace Corporation
Research Department - MS A08-35
ATTN: John E. A. Selby
Bethpage, NY 11714

Rome Air Development Center
ATTN: Documents Library
TSLD (Bette Smith)
Griffiss AFB, NY 13441

Dr. Roberto Vaglio-Laurin
Faculty of Arts and Science
Dept. of Applied Science
26-36 Stuyvesant Street
New York, NY 10003

Air Force Wright Aeronautical Laboratories/
Avionics Laboratory
ATTN: AFWAL/AARI-3 (Mr. Harold Geltmacher)
Wright-Patterson AFB, OH 45433

Air Force Wright Aeronautical Laboratories/
Avionics Laboratory
ATTN: AFWAL/AARI-3 (CPT William C. Smith)
Wright-Patterson AFB, OH 45433

Commandant
US Army Field Artillery School
ATTN: ATSF-CF-R (CPT James M. Watson)
Fort Sill, OK 73503

Commandant
US Army Field Artillery School
ATTN: ATSF-CD-MS
Fort Sill, OK 73503

Commandant
US Army Field Artillery School
ATTN: ATSF-CF-R
Fort Sill, OK 73503

Commandant
US Army Field Artillery School
ATTN: NOAA Liaison Officer
(CDR Jeffrey G. Carlen)
Fort Sill, OK 73503

Commandant
US Army Field Artillery School
Morris Swett Library
ATTN: Reference Librarian
Fort Sill, OK 73503

Commander
Naval Air Development Center
ATTN: Code 301 (Mr. George F. Eck)
Warminster, PA 18974

The University of Texas at El Paso
Electrical Engineering Department
ATTN: Dr. Joseph H. Pierluissi
El Paso, TX 79968

Commandant
US Army Air Defense School
ATTN: ATSA-CD-SC-A (CPT Charles T. Thorn)
Fort Bliss, TX 79916

Commander
HQ, TRADOC Cobmined Arms Test Activity
ATTN: ATCAT-OP-Q (CPT Henry C. Cobb, Jr.)
Fort Hood, TX 76544

Commander
HQ, TRADOC Combined Arms Test Activity
ATTN: ATCAT-SCI (Dr. Darrell W. Collier)
Fort Hood, TX 76544

Commander
US Army Dugway Proving Ground
ATTN: STEDP-MT-DA-L
Dugway, UT 84022

Commander
US Army Dugway Proving Ground
ATTN: STEDP-MT-DA-M (Mr. Paul E. Carlson)
Dugway, UT 84022

Commander
US Army Dugway Proving Ground
ATTN: STEDP-MT-DA-T (Mr. John Trethewey)
Dugway, UT 84022

Commander
US Army Dugway Proving Ground
ATTN: STEDP-MT-DA-T (Mr. William Peterson)
Dugway, UT 84022

Defense Documentation Center
ATTN: DDC-TCA
Cameron Station Bldg 5
Alexandria, VA 22314
12

Ballistic Missile Defense Program Office
ATTN: DACS-BMT (Colonel Harry F. Ennis)
5001 Eisenhower Avenue
Alexandria, VA 22333

Defense Technical Information Center
ATTN: DDA-2 (Mr. James E. Shafer)
Cameron Station, Bldg 5
Alexandria, VA 22314

Commander
US Army Materiel Development
& Readiness Command
ATTN: DRCBSI-EE (Mr. Albert Giambalvo)
5001 Eisenhower Avenue
Alexandria, VA 22333

Commander
US Army Materiel Development
& Readiness Command
ATTN: DRCLDC (Mr. James Bender)
5001 Eisenhower Avenue
Alexandria, VA 22333

Defense Advanced Rsch Projects Agency
ATTN: Steve Zakanyez
1400 Wilson Blvd
Arlington, VA 22209

Defense Advanced Rsch Projects Agency
ATTN: Dr. James Tegnelia
1400 Wilson Blvd
Arlington, VA 22209

Institute for Defense Analyses
ATTN: Mr. Lucien M. Biberman
400 Army-Navy Drive
Arlington, VA 22202

Institute for Defense Analyses
ATTN: Dr. Ernest Bauer
400 Army-Navy Drive
Arlington, VA 22202

Institute of Defense Analyses
ATTN: Dr. Hans G. Wolfhard
400 Army-Navy Drive
Arlingon, VA 22202

System Planning Corporation
ATTN: Mr. Daniel Friedman
1500 Wilson Boulevard
Arlington, VA 22209

System Planning Corporation
ATTN: COL Hank Shelton
1500 Wilson Boulevard
Arlington, VA 22209

US Army Intelligence & Security Command
ATTN: Edwin Speakman, Scientific Advisor
Arlington Hall Station
Arlington, VA 22212

Commander
US Army Operational Test
& Evaluation Agency
ATTN: CSTE-ED (Mr. Floyd I. Hill)
5600 Columbia Pike
Falls Church, VA 22041

Commander and Director
US Army Engineer Topographic Laboratories
ATTN: ETL-GS-A (Mr. Thomas Neidringhaus)
Fort Belvoir, VA 22060

Director
US Army Night Vision &
Electro-Optics Laboratory
ATTN: DELNV-L (Dr. Rudolf G. Buser)
Fort Belvoir, VA 22060

Director
US Army Night Vision &
Electro-Optics Laboratory
ATTN: DELNV-L (Dr. Robert S. Rodhe)
Fort Belvoir, VA 22060

Director
US Army Night Vision &
Electro-Optics Laboratory
ATTN: DELNV-VI (Mr. Joseph R. Moulton)
Fort Belvoir, VA 22060

Director
US Army Night Vision &
Electro-Optics Laboratory
ATTN: DELNV-VI (Luanne P. Obert)
Fort Belvoir, VA 22060

Director
US Army Night Vision
& Electro-Optics Laboratory
ATTN: DELNV-VI (Mr. Thomas W. Cassidy)
Fort Belvoir, VA 22060

Director
US Army Night Vision &
Electro-Optics Laboratory
ATTN: DELNV-VI (Mr. Richard J. Bergemann)
Fort Belvoir, VA 22060

Director
US Army Night Vision &
Electro-Optics Laboratory
ATTN: DELNV-VI (Dr. James A. Ratches)
Fort Belvoir, VA 22060

Commander
US Army Training & Doctrine Command
ATTN: ATCD-AN
Fort Monroe, VA 23651

Commander
US Army Training & Doctrine Command
ATTN: ATCD-AN-M
Fort Monroe, VA 23651

Commander
US Army Training & Doctrine Command
ATTN: ATCD-F-A (Mr. Chris O'Connor, Jr.)
Fort Monroe, VA 23651

Commander
US Army Training & Doctrine Command
ATTN: ATCD-IE-R (Mr. David M. Ingram)
Fort Monroe, VA 23651

Commander
US Army Training & Doctrine Command
ATTN: ATCD-M-I/ATCD-M-A
Fort Monroe, VA 23651

Commander
US Army Training & Doctrine Command
ATTN: ATDOC-TA (Dr. Marvin P. Pastel)
Fort Monroe, VA 23651

Department of the Air Force
OL-I, AWS
Fort Monroe, VA 23651

Department of the Air Force
HQS 5 Weather Wing (MAC)
ATTN: 5 WW/DN
Langley Air Force Base, VA 23655

Commander
US Army INSCOM/Quest Research Corporation
ATTN: Mr. Donald Wilmot
6845 Elm Street, Suite 407
McLean, VA 22101

General Research Corporation
ATTN: Dr. Ralph Zirkind
7655 Old Springhouse Road
McLean, VA 22102

Science Applications, Inc.
8400 Westpark Drive
ATTN: Dr. John E. Cockayne
McLean, VA 22102

US Army Nuclear & Chemical Agency
ATTN: MONA-WE (Dr. John A. Berberet)
7500 Backlick Road, Bldg 2073
Springfield, VA 22150

Director
US Army Signals Warfare Laboratory
ATTN: DELSW-EA (Mr. Douglas Harkleroad)
Vint Hill Farms Station
Warrenton, VA 22186

Director
US Army Signals Warfare Laboratory
ATTN: DELSW-OS (Dr. Royal H. Burkhardt)
Vint Hill Farms Station
Warrenton, VA 22186

Commander
US Army Cold Regions Test Center
ATTN: STECR-TD (Mr. Jerold Barger)
APO Seattle, WA 98733

HQDA (SAUS-OR/Hunter M. Woodall, Jr./
Dr. Herbert K. Fallin)
Rm 2E 614, Pentagon
Washington, DC 20301

COL Elbert W. Friday, Jr.
OUSDRE
Rm 3D 129, Pentagon
Washington, DC 20301

Defense Communications Agency
Technical Library Center
Code 222
Washington, DC 20305

Director
Defense Nuclear Agency
ATTN: Technical Library (Mrs. Betty Fox)
Washington, DC 20305

Director
Defense Nuclear Agency
ATTN: RAAE (Dr. Carl Fitz)
Washington, DC 20305

Director
Defense Nuclear Agency
ATTN: SPAS (Mr. Donald J. Kohler)
Washington, DC 20305

Defense Intelligence Agency
ATTN: DT/AC (LTC Robert Poplawski)
Washington, DC 20301

HQDA (DAMA-ARZ-D/Dr. Verderame)
Washington, DC 20310

HQDA (DAMI-ISP/Mr. Beck)
Washington, DC 20310

Department of the Army
Deputy Chief of Staff for
Operations and Plans
ATTN: DAMO-RQ
Washington, DC 20310

Department of the Army
Director of Telecommunications and
Command and Control
ATTN: DAMO-TCZ
Washington, DC 20310

Department of the Army
Assistant Chief of Staff for Intelligence
ATTN: DAMI-TS
Washington, DC 20310

HQDA (DAEN-RDM/Dr. de Percin)
Casimir Pulaski Building
20 Massachusetts Avenue
Room 6203
Washington, DC 20314

National Science Foundation
Division of Atmospheric Sciences
ATTN: Dr. Eugene W. Bierly
1800 G. Street, N.W.
Washington, DC 20550

Director
Naval Research Laboratory
ATTN: Code 4320 (Dr. Lothar H. Ruhnke)
Washington, DC 20375

Commanding Officer
Naval Research Laboratory
ATTN: Code 6009 (Dr. John MacCallum, Jr.)
Washington, DC 20375

Commanding Officer
Naval Research Laboratory
ATTN: Code 6530 (Mr. Raymond A. Patten)
Washington, DC 20375

Commanding Officer
Naval Research Laboratory
ATTN: Code 6533 (Dr. James A. Dowling)
Washington, DC 20375

ATMOSPHERIC SCIENCES RESEARCH PAPERS

1. Lindberg, J.D., "An Improvement to a Method for Measuring the Absorption Coefficient of Atmospheric Dust and other Strongly Absorbing Powders," ECOM-5565, July 1975.
2. Avara, Elton, P., "Mesoscale Wind Shears Derived from Thermal Winds," ECOM-5566, July 1975.
3. Gomez, Richard B., and Joseph H. Pierluissi, "Incomplete Gamma Function Approximation for King's Strong-Line Transmittance Model," ECOM-5567, July 1975.
4. Blanco, A.J., and B.F. Engebos, "Ballistic Wind Weighting Functions for Tank Projectiles," ECOM-5568, August 1975.
5. Taylor, Fredrick J., Jack Smith, and Thomas H. Pries, "Crosswind Measurements through Pattern Recognition Techniques," ECOM-5569, July 1975.
6. Walters, D.L., "*Crosswind Weighting Functions for Direct-Fire Projectiles*," ECOM-5570, August 1975.
7. Duncan, Louis D., "An Improved Algorithm for the Iterated Minimal Information Solution for Remote Sounding of Temperature," ECOM-5571, August 1975.
8. Robbiani, Raymond L., "Tactical Field Demonstration of Mobile Weather Radar Set AN TPS-41 at Fort Rucker, Alabama," ECOM-5572, August 1975.
9. Miers, B., G. Blackman, D. Langer, and N. Lorimier, "Analysis of SMS GOES Film Data," ECOM-5573, September 1975.
10. Manquero, Carlos, Louis Duncan, and Rufus Bruce, "An Indication from Satellite Measurements of Atmospheric CO2 Variability," ECOM-5574, September 1975.
11. Petracca, Carmine, and James D. Lindberg, "Installation and Operation of an Atmospheric Particulate Collector," ECOM-5575, September 1975.
12. Avara, Elton P., and George Alexander, "Empirical Investigation of Three Iterative Methods for Inverting the Radiative Transfer Equation," ECOM-5576, October 1975.
13. Alexander, George D., "A Digital Data Acquisition Interface for the SMS Direct Readout Ground Station — Concept and Preliminary Design," ECOM-5577, October 1975.
14. Cantor, Israel, "Enhancement of Point Source Thermal Radiation Under Clouds in a Nonattenuating Medium," ECOM-5578, October 1975.
15. Norton, Colburn, and Glenn Hoidale, "The Diurnal Variation of Mixing Height by Month over White Sands Missile Range, N.M," ECOM-5579, November 1975.
16. Avara, Elton P., "On the Spectrum Analysis of Binary Data," ECOM-5580, November 1975.
17. Taylor, Fredrick J., Thomas H. Pries, and Chao-Huan Huang, "Optimal Wind Velocity Estimation," ECOM-5581, December 1975.
18. Avara, Elton P., "Some Effects of Autocorrelated and Cross-Correlated Noise on the Analysis of Variance," ECOM-5582, December 1975.
19. Gillespie, Patti S., R.L. Armstrong, and Kenneth O. White, "The Spectral Characteristics and Atmospheric CO2 Absorption of the Ho:YLF Laser at 2.05μm," ECOM-5583, December 1975.
20. Novlan, David J. "An Empirical Method of Forecasting Thunderstorms for the White Sands Missile Range," ECOM-5584, February 1976.
21. Avara, Elton P., "Randomization Effects in Hypothesis Testing with Autocorrelated Noise," ECOM-5585, February 1976.
22. Watkins, Wendell R., "Improvements in Long Path Absorption Cell Measurement," ECOM-5586, March 1976.
23. Thomas, Joe, George D. Alexander, and Marvin Dubbin, "SATTEL An Army Dedicated Meteorological Telemetry System," ECOM-5587, March 1976.
24. Kennedy, Bruce W., and Delbert Bynum, "Army User Test Program for the RDT&E-XM-75 Meteorological Rocket," ECOM-5588, April 1976.

25. Barnett, Kenneth M., "A Description of the Artillery Meteorological Comparisons at White Sands Missle Range, October 1974 - December 1974 (PASS) - Prototype Artillery [Meteorological] Subsystem)," ECOM-5589, April 1976.
26. Miller, Walter B., "Preliminary Analysis of Fall-of-Shot From Project 'PASS'," ECOM-5590, April 1976.
27. Avara, Elton P., "Error Analysis of Minimum Information and Smith's Direct Methods for Inverting the Radiative Transfer Equation," ECOM-5591, April 1976.
28. Yee, Young P., James D. Horn, and George Alexander, "Synoptic Thermal Wind Calculations from Radiosonde Observations Over the Southwestern United States," ECOM-5592, May 1976.
29. Duncan, Louis D., and Mary Ann Seagraves, "Applications of Empirical Corrections to NOAA-4 VTPR Observations," ECOM-5593, May 1976.
30. Miers, Bruce T., and Steve Weaver, "Applications of Meterological Satellite Data to Weather Sensitive Army Operations,"ECOM-5594, May 1976.
31. Sharenow, Moses, "Redesign and Improvement of Balloon ML-566," ECOM-5595, June, 1976.
32. Hansen, Frank V., "The Depth of the Surface Boundary Layer," ECOM-5596, June 1976.
33. Pinnick, R.G., and E.B. Stenmark, "Response Calculations for a Commercial Light-Scattering Aerosol Counter," ECOM-5597, July 1976.
34. Mason, J., and G.B. Hoidale, "Visibility as an Estimator of Infrared Transmittance," ECOM-5598, July 1976.
35. Bruce, Rufus E., Louis D. Duncan, and Joseph H. Pierluissi, "Experimental Study of the Relationship Between Radiosonde Temperatures and Radiometric-Area Temperatures," ECOM-5599, August 1976.
36. Duncan, Louis D., "Stratospheric Wind Shear Computed from Satellite Thermal Sounder Measurements," ECOM-5800, September 1976.
37. Taylor, F., P. Mohan, P. Joseph and T. Pries, "An All Digital Automated Wind Measurement System," ECOM-5801, September 1976.
38. Bruce, Charles, "Development of Spectrophones for CW and Pulsed Radiation Sources," ECOM-5802, September 1976.
39. Duncan, Louis D., and Mary Ann Seagraves,"Another Method for Estimating Clear Column Radiances," ECOM-5803, October 1976.
40. Blanco, Abel J., and Larry E. Taylor, "Artillery Meteorological Analysis of Project Pass," ECOM-5804, October 1976.
41. Miller, Walter, and Bernard Engebos," A Mathematical Structure for Refinement of Sound Ranging Estimates," ECOM-5805, November, 1976.
42. Gillespie, James B., and James D. Lindberg, "A Method to Obtain Diffuse Reflectance Measurements from 1.0 to 3.0 μm Using a Cary 17I Spectrophotometer," ECOM-5806, November 1976.
43. Rubio, Roberto, and Robert O. Olsen,"A Study of the Effects of Temperature Variations on Radio Wave Absorption,"ECOM-5807, November 1976.
44. Ballard, Harold N., "Temperature Measurements in the Stratosphere from Balloon-Borne Instrument Platforms, 1968-1975," ECOM-5808, December 1976.
45. Monahan, H.H., "An Approach to the Short-Range Prediction of Early Morning Radiation Fog," ECOM-5809, January 1977.
46. Engebos, Bernard Francis, "Introduction to Multiple State Multiple Action Decision Theory and Its Relation to Mixing Structures," ECOM-5810, January 1977.
47. Low, Richard D.H.,"Effects of Cloud Particles on Remote Sensing from Space in the 10-Micrometer Infrared Region," ECOM-5811, January 1977.
48 Bonner, Robert S., and R. Newton, "Application of the AN/GVS-5 Laser Rangefinder to Cloud Base Height Measurements," ECOM-5812, February 1977.
49. Rubio, Roberto, "Lidar Detection of Subvisible Reentry Vehicle Erosive Atmospheric Material," ECOM-5813, March 1977.
50. Low, Richard D.H., and J.D. Horn, "Mesoscale Determination of Cloud Top Height: Problems and Solutions," ECOM-5814, March 1977.

51. Duncan, Louis D., and Mary Ann Seagraves, "Evaluation of the NOAA-4 VTPR Thermal Winds for Nuclear Fallout Predictions," ECOM-5815, March 1977.
52. Randhawa, Jagir S., M. Izquierdo, Carlos McDonald and Zvi Salpeter, "Stratospheric Ozone Density as Measured by a Chemiluminescent Sensor During the Stratcom VI-A Flight," ECOM-5816, April 1977.
53. Rubio, Roberto, and Mike Izquierdo, "Measurements of Net Atmospheric Irradiance in the 0.7- to 2.8-Micrometer Infrared Region," ECOM-5817, May 1977.
54. Ballard, Harold N., Jose M. Serna, and Frank P. Hudson Consultant for Chemical Kinetics, "Calculation of Selected Atmospheric Composition Parameters for the Mid-Latitude, September Stratosphere," ECOM-5818, May 1977.
55. Mitchell, J.D., R.S. Sagar, and R.O. Olsen, "Positive Ions in the Middle Atmosphere During Sunrise Conditions," ECOM-5819, May 1977.
56. White, Kenneth O., Wendell R. Watkins, Stuart A. Schleusener, and Ronald L. Johnson, "Solid-State Laser Wavelength Identification Using a Reference Absorber," ECOM-5820, June 1977.
57. Watkins, Wendell R., and Richard G. Dixon, "Automation of Long-Path Absorption Cell Measurements," ECOM-5821, June 1977.
58. Taylor, S.E., J.M. Davis, and J.B. Mason, "Analysis of Observed Soil Skin Moisture Effects on Reflectance," ECOM-5822, June 1977.
59. Duncan, Louis D. and Mary Ann Seagraves, "Fallout Predictions Computed from Satellite Derived Winds," ECOM-5823, June 1977.
60. Snider, D.E., D.G. Murcray, F.H. Murcray, and W.J. Williams, "Investigation of High-Altitude Enhanced Infrared Background Emissions" (U), SECRET, ECOM-5824, June 1977.
61. Dubbin, Marvin H. and Dennis Hall, "Synchronous Meteorlogical Satellite Direct Readout Ground System Digital Video Electronics," ECOM-5825, June 1977.
62. Miller, W., and B. Engebos, "A Preliminary Analysis of Two Sound Ranging Algorithms," ECOM-5826, July 1977.
63. Kennedy, Bruce W., and James K. Luers, "Ballistic Sphere Techniques for Measuring Atomspheric Parameters," ECOM-5827, July 1977
64. Duncan, Louis D., "Zenith Angle Variation of Satellite Thermal Sounder Measurements," ECOM-5828, August 1977.
65. Hansen, Frank V., "The Critical Richardson Number," ECOM-5829, September 1977.
66. Ballard, Harold N., and Frank P. Hudson (Compilers), "Stratospheric Composition Balloon-Borne Experiment," ECOM-5830, October 1977.
67. Barr, William C., and Arnold C. Peterson, "Wind Measuring Accuracy Test of Meteorological Systems," ECOM-5831, November 1977.
68. Ethridge, G.A. and F.V. Hansen, "Atmospheric Diffusion: Similarity Theory and Empirical Derivations for Use in Boundary Layer Diffusion Problems," ECOM-5832, November 1977.
69. Low, Richard D.H., "The Internal Cloud Radiation Field and a Technique for Determining Cloud Blackness," ECOM-5833, December 1977.
70. Watkins, Wendell R., Kenneth O. White, Charles W. Bruce, Donald L. Walters, and James D. Lindberg, "Measurements Required for Prediction of High Energy Laser Transmission," ECOM-5834, December 1977.
71. Rubio, Robert, "Investigation of Abrupt Decreases in Atmospherically Backscattered Laser Energy," ECOM-5835, December 1977.
72. Monahan, H.H. and R.M. Cionco, "An Interpretative Review of Existing Capabilities for Measuring and Forecasting Selected Weather Variables (Emphasizing Remote Means)," ASL-TR-0001, January 1978.
73. Heaps, Melvin G., "The 1979 Solar Eclipse and Validation of D-Region Models," ASL-TR-0002, March 1978.

74. Jennings, S.G., and J.B. Gillespie, "M.I.E. Theory Sensitivity Studies - The Effects of Aerosol Complex Refractive Index and Size Distribution Variations on Extinction and Absorption Coefficients Part II: Analysis of the Computational Results," ASL-TR-0003, March 1978.
75. White, Kenneth O. et al, "Water Vapor Continuum Absorption in the 3.5μm to 4.0μm Region," ASL-TR-0004, March 1978.
76. Olsen, Robert O., and Bruce W. Kennedy, "ABRES Pretest Atmospheric Measurements," ASL-TR-0005, April 1978.
77. Ballard, Harold N., Jose M. Serna, and Frank P. Hudson, "Calculation of Atmospheric Composition in the High Latitude September Stratosphere," ASL-TR-0006, May 1978.
78. Watkins, Wendell R. et al, "Water Vapor Absorption Coefficients at HF Laser Wavelengths," ASL-TR-0007, May 1978.
79. Hansen, Frank V., "The Growth and Prediction of Nocturnal Inversions," ASL-TR-0008, May 1978.
80. Samuel, Christine, Charles Bruce, and Ralph Brewer, "Spectrophone Analysis of Gas Samples Obtained at Field Site," ASL-TR-0009, June 1978.
81. Pinnick, R.G. et al., "Vertical Structure in Atmospheric Fog and Haze and its Effects on IR Extinction," ASL-TR-0010, July 1978.
82. Low, Richard D.H., Louis D. Duncan, and Richard B. Gomez, "The Microphysical Basis of Fog Optical Characterization," ASL-TR-0011, August 1978.
83. Heaps, Melvin G., "The Effect of a Solar Proton Event on the Minor Neutral Constituents of the Summer Polar Mesosphere," ASL-TR-0012, August 1978.
84. Mason, James B., "Light Attenuation in Falling Snow," ASL-TR-0013, August 1978.
85. Blanco, Abel J., "Long-Range Artillery Sound Ranging: "PASS" Meteorological Application," ASL-TR-0014, September 1978.
86. Heaps, M.G., and F.E. Niles, "Modeling the Ion Chemistry of the D-Region: A case Study Based Upon the 1966 Total Solar Eclipse," ASL-TR-0015, September 1978.
87. Jennings, S.G., and R.G. Pinnick, "Effects of Particulate Complex Refractive Index and Particle Size Distribution Variations on Atmospheric Extinction and Absorption for Visible Through Middle-Infrared Wavelengths," ASL-TR-0016, September 1978.
88. Watkins, Wendell R., Kenneth O. White, Lanny R. Bower, and Brian Z. Sojka, " Pressure Dependence of the Water Vapor Continuum Absorption in the 3.5- to 4.0 Micrometer Region," ASL-TR-0017, September 1978.
89. Miller, W.B., and B.F. Engebos, "Behavior of Four Sound Ranging Techniques in an Idealized Physical Enviroment," ASL-TR-0018, September 1978.
90. Gomez, Richard G., "Effectiveness Studies of the CBU-88/B Bomb, Cluster, Smoke Weapon" (U), CONFIDENTIAL ASL-TR-0019, September 1978.
91. Miller, August, Richard C. Shirkey, and Mary Ann Seagraves, "Calculation of Thermal Emission from Aerosols Using the Doubling Technique," ASL-TR-0020, November, 1978.
92. Lindberg, James D. et al., "*Measured Effects of Battlefield Dust and Smoke on* Visible, Infrared, and Millimeter Wavelengths Propagation: A Preliminary Report on Dusty Infrared Test-I (DIRT-I)," ASL-TR-0021, January 1979.
93. Kennedy, Bruce W., Arthur Kinghorn, and B.R. Hixon, "Engineering Flight Tests of Range Meteorological Sounding System Radiosonde," ASL-TR-0022, February 1979.
94. Rubio, Roberto, and Don Hoock, "Microwave Effective Earth Radius Factor Variability at Wiesbaden and Balboa," ASL-TR-0023, February 1979.
95. Low, Richard D.H., "A Theoretical Investigation of Cloud/Fog Optical Properties and Their Spectral Correlations," ASL-TR-0024, February 1979.

96. Pinnick, R.G., and H.J. Auvermann, "Response Characteristics of Knollenberg Light-Scattering Aerosol Counters," ASL-TR-0025, February 1979.
97. Heaps, Melvin G., Robert O. Olsen, and Warren W. Berning, "Solar Eclipse 1979, Atmospheric Sciences Laboratory Program Overview," ASL-TR-0026 February 1979.
98. Blanco, Abel J., "Long-Range Artillery Sound Ranging: 'PASS' GR-8 Sound Ranging Data," ASL-TR-0027, March 1979.
99. Kennedy, Bruce W., and Jose M. Serna, "Meteorological Rocket Network System Reliability," ASL-TR-0028, March 1979.
100. Swingle, Donald M., "Effects of Arrival Time Errors in Weighted Range Equation Solutions for Linear Base Sound Ranging," ASL-TR-0029, April 1979.
101. Umstead, Robert K., Ricardo Pena, and Frank V. Hansen, "KWIK: An Algorithm for Calculating Munition Expenditures for Smoke Screening/Obscuration in Tactical Situations," ASL-TR-0030, April 1979.
102. D'Arcy, Edward M., "Accuracy Validation of the Modified Nike Hercules Radar," ASL-TR-0031, May 1979.
103. Rodriguez, Ruben, "Evaluation of the Passive Remote Crosswind Sensor," ASL-TR-0032, May 1979.
104. Barber, T.L., and R. Rodgriquez, "Transit Time Lidar Measurement of Near-Surface Winds in the Atmosphere," ASL-TR-0033, May 1979.
105. Low, Richard D.H., Louis D. Duncan, and Y.Y. Roger R. Hsiao, "Microphysical and Optical Properties of California Coastal Fogs at Fort Ord," ASL-TR-0034, June 1979.
106. Rodriguez, Ruben, and William J. Vechione, "Evaluation of the Saturation Resistant Crosswind Sensor," ASL-TR-0035, July 1979.
107. Ohmstede, William D., "The Dynamics of Material Layers," ASL-TR-0036, July 1979.
108. Pinnick, R.G., S.G. Jennings, Petr Chylek, and H.J. Auvermann "Relationships between IR Extinction, Absorption, and Liquid Water Content of Fogs," ASL-TR-0037, August 1979.
109. Rodriguez, Ruben, and William J. Vechione, "Performance Evaluation of the Optical Crosswind Profiler," ASL-TR-0038, August 1979.
110. Miers, Bruce T., "Precipitation Estimation Using Satellite Data" ASL-TR-0039, September 1979.
111. Dickson, David H., and Charles M. Sonnenschein, "Helicopter Remote Wind Sensor System Description," ASL-TR-0040, September 1979.
112. Heaps, Melvin, G., and Joseph M. Heimerl, "Validation of the Dairchem Code, I: Quiet Midlatitude Conditions," ASL-TR-0041, September 1979.
113. Bonner, Robert S., and William J. Lentz, "The Visioceilometer: A Portable Cloud Height and Visibility Indicator," ASL-TR-0042, October 1979.
114. Cohn, Stephen L., "The Role of Atmospheric Sulfates in Battlefield Obscurations," ASL-TR-0043, October 1979.
115. Fawbush, E.J. et al, "Characterization of Atmospheric Conditions at the High Energy Laser System Test Facility (HELSTF), White Sands Missile Range, New Mexico, Part I, 24 March to 8 April 1977," ASL-TR-0044, November 1979
116. Barber, Ted L., "Short-Time Mass Variation in Natural Atmospheric Dust," ASL-TR-0045, November 1979
117. Low, Richard D.H., "Fog Evolution in the Visible and Infrared Spectral Regions and its Meaning in Optical Modeling," ASL-TR-0046, December 1979
118. Duncan, Louis D. et al, "The Electro-Optical Systems Atmospheric Effects Library, Volume I: Technical Documentation, ASL-TR-0047, December 1979.
119. Shirkey, R. C. et al, "Interim E-O SAEL, Volume II, Users Manual," ASL-TR-0048, December 1979.
120. Kobayashi, H.K., "Atmospheric Effects on Millimeter Radio Waves," ASL-TR-0049, January 1980.
121. Seagraves, Mary Ann and Duncan, Louis D., "An Analysis of Transmittances Measured Through Battlefield Dust Clouds," ASL-TR-0050, February, 1980.

122. Dickson, David H., and Jon E. Ottesen, "Helicopter Remote Wind Sensor Flight Test," ASL-TR-0051, February 1980.
123. Pinnick, R. G., and S. G. Jennings, "Relationships Between Radiative Properties and Mass Content of Phosphoric Acid, HC, Petroleum Oil, and Sulfuric Acid Military Smokes," ASL-TR-0052, April 1980.
124. Hinds, B. D., and J. B. Gillespie, "Optical Characterization of Atmospheric Particulates on San Nicolas Island, California," ASL-TR-0053, April 1980.
125. Miers, Bruce T., "Precipitation Estimation for Military Hydrology," ASL-TR-0054, April 1980.
126. Stenmark, Ernest B., "Objective Quality Control of Artillery Computer Meteorological Messages," ASL-TR-0055, April 1980.
127. Duncan, Louis D., and Richard D. H. Low, "Bimodal Size Distribution Models for Fogs at Meppen, Germany, " ASL-TR-0056, April 1980.
128. Olsen, Robert O., and Jagir S. Randhawa, "The Influence of Atmospheric Dynamics on Ozone and Temperature Structure," ASL-TR-0057, May 1980.
129. Kennedy, Bruce W., et al, "Dusty Infrared Test-II (DIRT-II) Program," ASL-TR-0058, May 1980.
130. Heaps, Melvin G., Roberts O. Olsen, Warren Berning, John Cross, and Arthur Gilcrease, "1979 Solar Eclipse, Part I - Atmospheric Sciences Laboratory Field Program Summary," ASL-TR-0059, May 1980.
131. Miller, Walter B., "User's Guide for Passive Target Acquisition Program Two (PTAP-2)," ASL-TR-0060, June 1980.
132. Holt, E. H., H. H. Monahan, and E. J. Fawbush, "Atmospheric Data Requirements for Battlefield Obscuration Applications," ASL-TR-0061, June 1980.
133. Shirkey, Richard C., August Miller, George H. Goedecke, and Yugal Behl, "Single Scattering Code AGAUSX: Theory, Applications, Comparisons, and Listing," ASL-TR-0062, July 1980.
134. Sojka, Brain Z., and Kenneth O. White, "Evaluation of Specialized Photoacoustic Absorption Chambers for Near-millimeter Wave (NMMW) Propagation Measurements," ASL-TR-0063, August 1980.
135. Bruce, Charles W., Young Paul Yee, and S. G. Jennings, "In Situ Measurement of the Ratio of Aerosol Absorption to Extinction Coefficient," ASL-TR-0064, August 1980.
136. Yee, Young Paul, Charles W. Bruce, and Ralph J. Brewer, "Gaseous/Particulate Absorption Studies at WSMR using Laser Sourced Spectrophones," ASL-TR-0065, June 1980.
137. Lindberg, James D., Radon B. Loveland, Melvin Heaps, James B. Gillespie, and Andrew F. Lewis, "Battlefield Dust and Atmospheric Characterization Measurements During West German Summertime Conditions in Support of Grafenwohr Tests," ASL-TR-0066, September 1980.
138. Vechione, W. J., "Evaluation of the Environmental Instruments, Incorporated Series 200 Dual Component Wind Set," ASL-TR-0067, September 1980.
139. Bruce, C. W., Y. P. Yee, B. D. Hinds, R. G. Pinnick, R. J. Brewer, and J. Minjares, "Initial Field Measurements of Atmospheric Absorption at 9μM to 11μM Wavelengths, " ASL-TR-0068, October 1980.
140. Heaps, M. G., R. O. Olsen, K. D. Baker, D. A. Burt, L. C. Howlett, L. L. Jensen, E. F. Pound, and G. D. Allred, "1979 Solar Eclipse: Part II Initial Results for Ionization Sources, Electron Density, and Minor Neutral Constituents," ASL-TR-0069, October 1980.

★U.S. GOVERNMENT PRINTING OFFICE: 1980-0-777-026/5

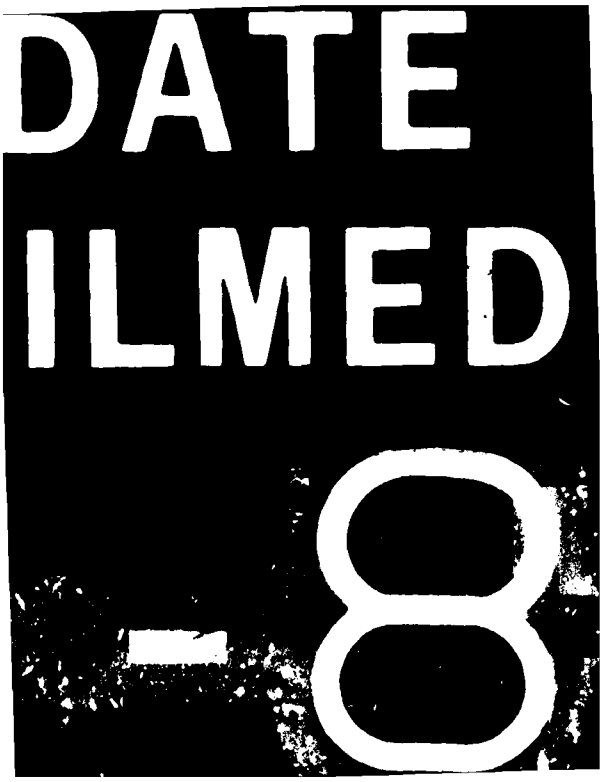
DATE
ILMED
8